Int J Fract (2008) 149:143–173
DOI 10.1007/s10704-008-9234-2

ORIGINAL PAPER

Failure initiation at a blunt V-notch tip under mixed mode loading

Elad Priel · Zohar Yosibash · Dominique Leguillon

Received: 20 December 2007 / Accepted: 21 May 2008 / Published online: 8 July 2008

Abstract A criterion to predict crack onset at a sharp V-notch tip in homogeneous brittle materials under a mixed-mode loading was presented and validated by experimental observations in a previous paper by the authors. This criterion slightly underestimates the experimental loads causing failure which is attributed to a small notch tip radius that blunts the sharp corner. This discrepancy is rigorously analyzed mathematically in this paper by means of matched asymptotics involving 2 small parameters: a micro-crack increment length and the notch tip radius. A correction is brought to the initial prediction and a better agreement is obtained with experiments on PMMA notched specimens.

Keywords Failure initiation · Mixed-mode fracture · Generalized stress intensity factors · V-notch · U-notch

Nomenclature

A_1, A_2	Generalized stress intensity factors (GSIFs), mode I and mode II, associated with the sharp V-notch
A_{1c}, A_{1c}^{blunt}	Critical mode I GSIF for sharp/blunt V-notch
α_1, α_2	Sharp V-notch singularity exponents
λ, G	The two Lamé constants
E, ν	Young modulus and Poisson ratio
G_c, σ_c, K_{Ic}	Fracture toughness, stress at brittle failure and plane-strain critical SIF
ℓ, ℓ_0	Crack length and critical crack length at the V-notch tip

E. Priel · Z. Yosibash (✉)
Department of Mechanical Engineering, Pearlstone Center for Aeronautical Engineering Studies, Ben-Gurion University of the Negev, Beer-Sheva 84105, Israel
e-mail: zohary@bgu.ac.il

D. Leguillon
LMM - CNRS UMR7607, Universite Pierre et Marie Curie, 75252 Paris Cedex 05, France
e-mail: dol@ccr.jussieu.fr

r, ρ	The radius measured from the V-notch tip in the outer and inner domains
θ	Angle measured from the horizontal axis in the inner and outer domains
θ^*	$\theta - \pi/2$
$\delta\Pi$	Change in potential energy due to the presence of a crack at the V-notch tip
a, μ	V-notch tip radius and normalized crack length $\mu = \ell/a$
ω	Solid opening angle of the V-notch
$\Omega^0_\infty, \Omega^\mu_\infty$	Inner domain without/with a crack
$\boldsymbol{u}, \boldsymbol{\sigma}$	Radial and tangential displacement vector and stress tensor
$\boldsymbol{u}^a(0), \boldsymbol{u}^a(\mu)$	Displacements vector for the blunt V-notch without/with the presence of a crack
$\boldsymbol{v}_1, \boldsymbol{v}_2$	Mode I and II expansion terms of the displacements vector in the inner domain
$\hat{\boldsymbol{v}}^{(1)}, \hat{\boldsymbol{v}}^{(2)}$	Mode I and II expansion terms of the displacements vector in the inner domain with finite strain energy
$\boldsymbol{u}(0,0)$	V-notch tip displacement vector
$\mathcal{L}$	The 2-D plane strain elasticity Navier operator
$\mathcal{T}$	The traction operator
$g(\rho)$	Cutoff function
Ψ	Path integral defined in (29)
Γ_∞	The circular boundary of the inner domain at $\rho \to \infty$
$H_{ij}(\mu,\theta), H_{ij}(0)$	Functions used to compute potential energy in cracked/uncracked domain with rounded V-notch tip
ΔH_{ij}	$H_{ij}(\mu,\theta) - H_{ij}(0)$
m	Mode mixity: $m = \frac{A_2}{A_1} a^{\alpha_2 - \alpha_1}$
σ_n	Normal stress
$\bar{\bullet}$	Quantities associated with the sharp V-notch
h^{mixed}, H^{mixed}	Correction factors for the computation of A_{Ic}

1 Introduction

The Leguillon criterion for the prediction of the failure load and crack initiation angle at the tip of a *sharp* V-notch in an elastic brittle isotropic material under mixed-mode (tension and shear) loading was developed and validated by experimental observations in Yosibash et al. (2006). Due to the assumption of the sharp V-notch tip, the predicted failure load was underestimated, and a correction to the failure criterion, taking into consideration the rounded V-notch tip is required. Herein, we extend the failure criterion in Yosibash et al. (2006) for blunt notches (having a small radius at the V-notch tip) under mixed mode loading (see notations in Fig. 1). The asymptotic analysis in Leguillon and Yosibash (2003) is revisited and a rigorous mathematical analysis is provided. Experimental observations on PMMA (polymer) blunt V-notched specimens are utilized to demonstrate the validity of the revised Leguillon criterion for predicting failure loads in domains containing rounded V-notch tips under a mixed mode loading.

Reliable prediction of the failure initiation instance (crack formation) in the vicinity of V-notch tips is a topic of active research and interest. At sharp V-notch tips the stress tensor is infinity under the assumption of linear elasticity (a particular case is a crack tip when the V-notch angle is 2π). Several failure criteria have been proposed for *sharp* V-notches in

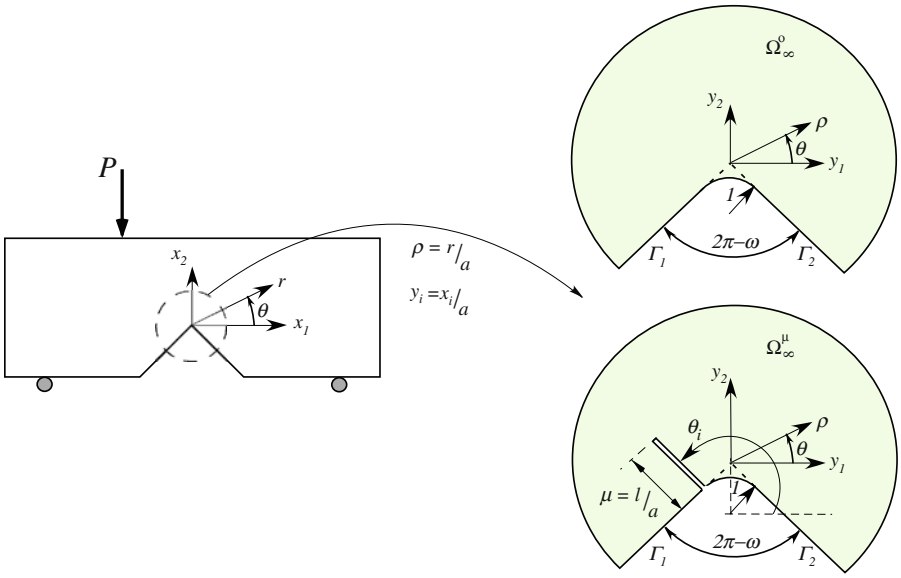

Fig. 1 Outer and inner expansion domains

brittle materials as the Leguillon failure criterion (Leguillon 2002; Leguillon et al. 2003), validated in Yosibash et al. (2004) for mode I loading and extended for mixed mode loading and validated by experimental observations in Yosibash et al. (2006). Leguillon's failure criterion has been extended for blunt notch tips under mode I loading in Leguillon and Yosibash (2003).

Prediction of the load that initiates failures in the vicinity of *blunt* notch tips attracted extensive research efforts in the past couple of years. In Leguillon and Yosibash (2003) rounded V-notches under mode I loading were considered whereas the cohesive zone model was applied in Gomez and Elices (2004) as a failure criterion for rounded V-notched or U-notched specimens under mode I loading, showing good correlation with many experimental observations. In Lazzarin and Berto (2005) the SED failure criterion was revised to incorporate the influence of a V-notch radius under Mode I loading and good correlation to some experimental observation is reported, where in Gomez et al. (2007) the SED criterion is extended to predict the static strength of U-notched specimens under mixed mode conditions due to combined bending and shear loads.

In Sect. 2 we derive an asymptotic analysis of the displacements in the vicinity of a *blunt* V-notch tip having a radius a with and without a crack of length ℓ. Based on this expansion, we derive an expression for the difference in potential energy (domain without a crack and with a crack in the vicinity of the rounded notch) without having to actually solve the cracked domain. This expression is used in Sect. 3 to reformulate Leguillon's failure criterion for mixed mode loading that takes into consideration a blunt V-notch tip. The various quantities required for the failure criterion and their verification are provided in Sect. 5. Finally, we validate the failure criterion by some experimental observations on PMMA specimens containing blunt V-notches under mixed mode loading in Sect. 6, and summarize our paper by Conclusions in Sect. 7.

2 Inner and outer expansions of the elastic solution

The corner-stone of the failure criterion (Leguillon 2002; Yosibash et al. 2006) is the postulate that a finite crack of length ℓ_0 has to be instantaneously created so to satisfy both the strength and toughness requirements. These two requirements which have to hold simultaneously at the instance of failure, state that the normal stress along a hypothetical crack length ℓ is larger than σ_c and at the same time the energy release rate for same crack length ℓ is equal the fracture toughness:

$$\sigma_n(\ell) = \sigma_c, \quad and \quad \frac{-\delta\Pi}{\ell} = G_c.$$

The crack is assumed to be orthogonal to the free surface, i.e. orthogonal to the principal stress, because the other two stress components vanish on the surface.

The difference in potential energy $(-\delta\Pi)$ between the state of a non-existing crack at the V-notch tip and the state of the presence of a crack of length ℓ_0 has to be computed:

$$-\delta\Pi \stackrel{\text{def}}{=} -(\Pi(\ell_0) - \Pi(\ell = 0)) \tag{1}$$

By an asymptotic analysis we proved (Yosibash et al. 2006) that for a sharp V-notch tip:

$$\begin{aligned} -\delta\Pi = -(\Pi(\ell_0) - \Pi(0)) = A_1^2 H_{11}(\ell_0, \theta_0)\ell_0^{2\alpha_1} + A_1 A_2 H_{12}(\ell_0, \theta_0)\ell_0^{\alpha_1+\alpha_2} \\ + A_2^2 H_{22}(\ell_0, \theta_0)\ell_0^{2\alpha_2} + \cdots \end{aligned} \tag{2}$$

where $-\delta\Pi$ is expressed in terms of A_i (the generalized stress intensity factors—see (3)–(5)), ℓ_0 and newly defined "Geometrical factors" named H_{ij} which are addressed in the sequel. Herein, we wish to find correction factors to $\delta\Pi$ so to account for the rounded V-notch tip.

We denote by $\mathcal{L}$ the Navier-Lamé operator (equilibrium equation in terms of displacements), and by $\mathcal{T}$ the traction operator.

2.1 Outer expansions of the elastic solution: sharp V-notch

For a small crack of length ℓ at the rounded V-notch tip, having a small radius a, one may consider the domain Ω of interest (shown in the left of Fig. 1) as if it has a sharp V-notch with no crack. The displacements and stresses in the vicinity of a traction free V-notch tip can be expressed by an asymptotic series which is provided in this section. In the literature (see Szabó and Babuška 1988 for example) the asymptotic series is usually expressed in a cylindrical coordinate system which is rotated by $\pi/2$ radians in respect to the coordinate system shown in Fig. 1. To distinguish between the two coordinate systems the one used in this section is marked with an asterisk, i.e. $\theta^* = \theta - \pi/2$, see Fig. 2. In the following we use either θ or θ^* as convenient.

The displacements in the vicinity of the sharp V-notch tip are expressed as a series, see e.g. Williams (1952), in which the first three terms are given by:

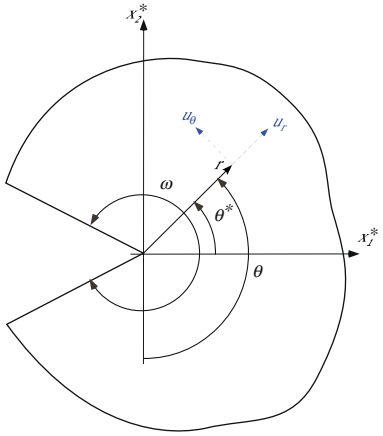

Fig. 2 The coordinate system at the V-notched tip for the outer expansion

$$\boldsymbol{u}(r,\theta) \overset{\text{def}}{=} \begin{Bmatrix} u_r \\ u_\theta \end{Bmatrix} = \boldsymbol{u}(0,0) + A_1 r^{\alpha_1} \begin{Bmatrix} \left[\cos(1+\alpha_1)\theta^* + \frac{[\lambda+3G-\alpha_1(\lambda+G)]}{(\lambda+G)(1-\alpha_1)} \frac{\sin[\omega(1+\alpha_1)/2]}{\sin[\omega(1-\alpha_1)/2]} \cos(1-\alpha_1)\theta^*\right] / \left(2G\alpha_1 \sigma^I_{\theta\theta}(\theta^*=0)\right) \\ \left[-\sin(1+\alpha_1)\theta^* - \frac{[\lambda+3G+\alpha_1(\lambda+G)]}{(\lambda+G)(1-\alpha_1)} \frac{\sin[\omega(1+\alpha_1)/2]}{\sin[\omega(1-\alpha_1)/2]} \sin(1-\alpha_1)\theta^*\right] / \left(2G\alpha_1 \sigma^I_{\theta\theta}(\theta^*=0)\right) \end{Bmatrix} \tag{3}$$

$$+ A_2 r^{\alpha_2} \begin{Bmatrix} \left[\sin(1+\alpha_2)\theta^* + \frac{[\lambda+3G-\alpha_2(\lambda+G)]}{(\lambda+G)(1+\alpha_2)} \frac{\sin[\omega(1+\alpha_2)/2]}{\sin[\omega(1-\alpha_2)/2]} \sin(1-\alpha_2)\theta^*\right] / \left(2G\alpha_2 \sigma^{II}_{r\theta}(\theta^*=0)\right) \\ \left[\cos(1+\alpha_2)\theta^* + \frac{[\lambda+3G+\alpha_2(\lambda+G)]}{(\lambda+G)(1+\alpha_2)} \frac{\sin[\omega(1+\alpha_2)/2]}{\sin[\omega(1-\alpha_2)/2]} \cos(1-\alpha_2)\theta^*\right] / \left(2G\alpha_2 \sigma^{II}_{r\theta}(\theta^*=0)\right) \end{Bmatrix}$$
$$+ \cdots \overset{\text{def}}{=} \boldsymbol{u}(0,0) + \sum_i A_i r^{\alpha_i} \boldsymbol{u}^{(i)}(\theta^*) \tag{4}$$

where $\boldsymbol{u}(0,0)$ is the rigid body displacement of the V-notch tip and the corresponding first two terms of the stress tensor in polar coordinates are:

$$\boldsymbol{\sigma} = \begin{Bmatrix} \sigma_{rr} \\ \sigma_{\theta\theta} \\ \sigma_{r\theta} \end{Bmatrix} = A_1 r^{\alpha_1 - 1} \begin{Bmatrix} \left[\cos(1+\alpha_1)\theta^* + \frac{(3-\alpha_1)}{(1-\alpha_1)} \frac{\sin[\omega(1+\alpha_1)/2]}{\sin[\omega(1-\alpha_1)/2]} \cos(1-\alpha_1)\theta^*\right] / \sigma^I_{\theta\theta}(\theta^*=0) \\ \left[-\cos(1+\alpha_1)\theta^* + \frac{(1+\alpha_1)}{(1-\alpha_1)} \frac{\sin[\omega(1+\alpha_1)/2]}{\sin[\omega(1-\alpha_1)/2]} \cos(1-\alpha_1)\theta^*\right] / \sigma^I_{\theta\theta}(\theta^*=0) \\ \left[-\sin(1+\alpha_1)\theta^* + \frac{\sin[\omega(1+\alpha_1)/2]}{\sin[\omega(1-\alpha_1)/2]} \sin(1-\alpha_1)\theta^*\right] / \sigma^I_{\theta\theta}(\theta^*=0) \end{Bmatrix}$$

$$+A_2 r^{\alpha_2-1}\left\{\begin{array}{c}\left[\sin(1+\alpha_2)\theta^*+\frac{(3-\alpha_2)}{(1+\alpha_2)}\frac{\sin[\omega(1+\alpha_2)/2]}{\sin[\omega(1-\alpha_2)/2]}\sin(1-\alpha_2)\theta^*\right]/\sigma_{r\theta}^{II}(\theta^*=0)\\ \left[-\sin(1+\alpha_2)\theta^*+\frac{\sin[\omega(1+\alpha_2)/2]}{\sin[\omega(1-\alpha_2)/2]}\sin(1-\alpha_2)\theta^*\right]/\sigma_{r\theta}^{II}(\theta^*=0)\\ \left[\cos(1+\alpha_2)\theta^*-\frac{(1-\alpha_2)}{(1+\alpha_2)}\frac{\sin[\omega(1+\alpha_2)/2]}{\sin[\omega(1-\alpha_2)/2]}\cos(1-\alpha_2)\theta^*\right]/\sigma_{r\theta}^{II}(\theta^*=0)\end{array}\right\} \tag{5}$$

In (3–5) we have used the following notations:

$$\sigma_{\theta\theta}^{I}(\theta^*=0)\overset{\text{def}}{=}\frac{(1+\alpha_1)}{(1-\alpha_1)}\frac{\sin[\omega(1+\alpha_1)/2]}{\sin[\omega(1-\alpha_1)/2]}-1 \tag{6}$$

$$\sigma_{r\theta}^{II}(\theta^*=0)\overset{\text{def}}{=}1-\frac{(1-\alpha_2)}{(1+\alpha_2)}\frac{\sin[\omega(1+\alpha_2)/2]}{\sin[\omega(1-\alpha_2)/2]} \tag{7}$$

in order to normalize the "eigen-stresses" so that for mode I

$$\sigma_{\theta\theta}^{I}(\theta^*=0)=1$$

and for mode II:

$$\sigma_{r\theta}^{II}(\theta^*=0)=1$$

then $\sigma_{\theta\theta}(r,\theta^*=0)=A_1 r^{\alpha_1-1}$ and $\sigma_{r\theta}(r,\theta^*=0)=A_2 r^{\alpha_2-1}$. The two "eigen-values" α_1 and α_2 are the smallest roots of the characteristic equations;

$$\sin(\alpha_1\omega)+\alpha_1\sin(\omega)=0 \tag{8}$$

$$\sin(\alpha_2\omega)-\alpha_2\sin(\omega)=0 \tag{9}$$

For a crack ($\omega=2\pi$) the Eqs. 8 and 9 are identical and the first two roots are real and simple $\alpha_1=\alpha_2=1/2$. In this case the "classical" mode I and II stresses and displacements for a crack, well known in fracture mechanics (Kanninen and Popelar 1985), are obtained and the coefficients A_1 and A_2 are related to the stress intensity factor: $A_1=K_I/\sqrt{2\pi}$, $A_2=K_{II}/\sqrt{2\pi}$. When $\omega\neq 2\pi$, then not all roots are real and multiple roots may exist. From the engineering viewpoint, V-notch solid angles up to $\frac{4\pi}{3}$ (240°) are of greatest importance and in this cases the smallest roots are real—see a summary in Table 1.

For a V-notch solid angle smaller than 1.43028π (257.45°), then $\alpha_2>1$ and the mode II stress components are bounded, whereas mode I stress components are bounded for $\omega<\pi$.

2.2 Asymptotic inner expansion for a rounded V-notch without a crack

To obtain the asymptotic expansion of the solution in the vicinity of a rounded V-notch tip having a radius a, we "zoom in" at the tip by performing a coordinate transformation: $\rho=r/a$ obtaining an unbounded "inner domain" denoted by Ω_∞°—see right top Fig. 1. In the crack free inner domain the solution is donated by $u^a(0)$ and may be represented as:

$$\boldsymbol{u}^a(0)=F_0(a)\boldsymbol{v}_0(\rho,\theta,0)+F_1(a)\boldsymbol{v}_1(\rho,\theta,0)+F_2(a)\boldsymbol{v}_2(\rho,\theta,0)+\cdots \tag{10}$$

Table 1 First two eigen-values for selected angles ω

Solid angle ω	2π (crack)	$\frac{11\pi}{6}$ (330°)	$\frac{7\pi}{4}$ (315°)	$\frac{5\pi}{3}$ (300°)	$\frac{3\pi}{2}$ (270°)	$\frac{4\pi}{3}$ (240°)
α_1	1/2	0.5014530	0.5050097	0.5122214	0.5444837	0.6157311
α_2	1/2	0.5981918	0.6597016	0.7309007	0.9085292	1.148913

with $\lim_{a\to 0}\frac{F_{i+1}(a)}{F_i(a)}=0$ and where 0 denotes the uncracked solution. Away from the notch tip the solution must match the V-notch solution $\boldsymbol{u}=\boldsymbol{u}(0,0)+A_i r^{\alpha_i}\boldsymbol{u}^{(i)}(\theta)$. We may match each term in (10) as $\rho\to\infty$ with the known outer solution obtaining:

$$\boldsymbol{u}^a(0)=\boldsymbol{u}(0,0)+A_1 a^{\alpha_1}\boldsymbol{v}_1(\rho,\theta,0)+A_2 a^{\alpha_2}\boldsymbol{v}_2(\rho,\theta,0)+\cdots \tag{11}$$

with $\boldsymbol{v}_i(\rho,\theta,0)\sim\rho^{\alpha_i}\boldsymbol{u}^{(i)}$ as $\rho\to\infty$, where $\sim$ means "behaves like".

There is a conceptual difficulty to solve for $\boldsymbol{v}_i(\rho,\theta,0)$ by finite element methods for example, because the strain energy of $\boldsymbol{v}_i(\rho,\theta,0)$ is unbounded in an infinite domain. Therefore, we may represent:

$$\boldsymbol{v}_i(\rho,\theta,0)=g(\rho)\times\rho^{\alpha_i}\boldsymbol{u}^{(i)}+\hat{\boldsymbol{v}}^{(i)}(0) \tag{12}$$

where $g(\rho)$ is a cutoff function which equals to 1 for $\rho\geq\rho_2$ and equals 0 for $\rho\leq\rho_1$, and $\hat{\boldsymbol{v}}^{(i)}(0)$ is a correction to the displacement field accounting for the notch blunting. In this case one may solve for $\hat{\boldsymbol{v}}^{(i)}(0)$ and thereafter obtain $\boldsymbol{v}_i(\rho,\theta,0)$. Note that $\hat{\boldsymbol{v}}^{(i)}(0)\to 0$ as $\rho\to\infty$. The cutoff function $g(\rho)$ is mandatory because the eigen-solution $\rho^{\alpha_i}\boldsymbol{u}^{(i)}$ is not valid outside of the sector $(\pi-\omega)/2<\theta<(\pi+\omega)/2$ in the vicinity of the rounding and the stresses associated with $\hat{\boldsymbol{v}}^{(i)}(0)$ should be finite as ρ approaches zero. In our analysis we chose:

$$g(\rho)=\begin{cases}0 & \rho\leq\rho_1\\ 1-3\left(\frac{\rho-\rho_2}{\rho_1-\rho_2}\right)^2+2\left(\frac{\rho-\rho_2}{\rho_1-\rho_2}\right)^3 & \rho_1<\rho<\rho_2\\ 1 & \rho\geq\rho_2\end{cases} \tag{13}$$

$\hat{\boldsymbol{v}}^{(i)}(0)$ is obtained by solving the elastic problem in the inner unbounded domain Ω°_{∞} (see for definition of the different boundaries Fig. 3(left)):

$$\begin{aligned}\mathcal{L}(\boldsymbol{u}^a(0)) &= \mathcal{L}(g(\rho)\rho^{\alpha_i}\boldsymbol{u}^{(i)}(\theta))+\mathcal{L}(\hat{\boldsymbol{v}}^{(i)}(0))=0\\ &\Rightarrow \mathcal{L}(\hat{\boldsymbol{v}}^{(i)}(0))=0 \quad in\ \Omega^{\circ}_{\infty}-[\rho_1<\rho<\rho_2]\\ &\Rightarrow \mathcal{L}(\hat{\boldsymbol{v}}^{(i)}(0))=-\rho^{\alpha_i}\boldsymbol{u}^{(i)}(\theta)\times\mathcal{L}\,(g(\rho)) \quad in\ [\rho_1<\rho<\rho_2] \qquad (14)\\ \mathcal{T}(\boldsymbol{u}^a(0)) &= \mathcal{T}(g(\rho)\rho^{\alpha_i}\boldsymbol{u}^{(i)}(\theta))+\mathcal{T}(\hat{\boldsymbol{v}}^{(i)}(0)))=0\\ &\Rightarrow \mathcal{T}(\hat{\boldsymbol{v}}^{(i)}(0)))=0 \quad on\ \Gamma_1,\Gamma_2,\Gamma_5 \qquad (15)\\ &\Rightarrow \mathcal{T}(\hat{\boldsymbol{v}}^{(i)}(0)))=-\rho^{\alpha_i}\boldsymbol{u}^{(i)}(\theta)\mathcal{T}(g(\rho)) \quad on\ \Gamma_3,\Gamma_4 \qquad (16)\end{aligned}$$

On Γ_∞, i.e. for $\rho\to\infty$, according to (12) one has to enforce $\hat{\boldsymbol{v}}^{(i)}(0)\to 0$. I.e. taking in practice a domain with a very large outer boundary, homogeneous Dirichlet boundary conditions are prescribed on Γ_∞.

Remark 1 For an isotropic material, the elasticity operator $\mathcal{L}$ when operating on an eigen-solution $\rho^{\alpha_i}\boldsymbol{u}^{(i)}(\theta)$ is identically zero (formally) in the entire domain: $\mathcal{L}(\rho^{\alpha_i}\boldsymbol{u}^{(i)}(\theta))\equiv 0$ (also in the sub-domain bounded by the circular boundary of radius 1 and the sharp V-notch). Also, since the eigen-solution satisfies the boundary conditions on the two straight lines that intersect at the V-notch tip, then $\mathcal{T}(\rho^{\alpha_i}\boldsymbol{u}^{(i)}(\theta))\big|_{\theta=(\pi-\omega)/2,(\pi+\omega)/2}\equiv 0$.

Remark 2 For the uncracked case, the stress field can be alternatively computed using the analytical approximation proposed by Lazzarin and Tovo (1996). Nevertheless, it does not extend to the cracked case (Sect. 2.3) and moreover, the displacement field is required in addition to the stress field in both cases (Sect. 2.4). Thus, for simplicity, the same numerical procedure presented herein is carried out in the two cases.

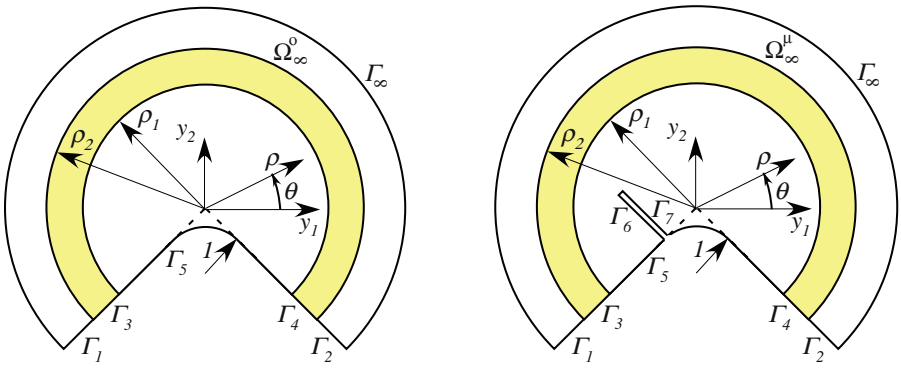

Fig. 3 Inner expansion domain Ω°_{∞} (left) and Ω^{μ}_{∞} (right)

2.3 Asymptotic inner expansion for a rounded V-notch with a crack

We conduct a second expansion to obtain the solution for the cracked blunt notch. We again expand with respect to a and now denote by $\mu = \frac{\ell}{a}$ the new dimensionless crack length at the blunt tip. Using the same matching procedure one obtains:

$$\boldsymbol{u}^a(\mu) = \boldsymbol{u}(0,0) + A_1 a^{\alpha_1}(\boldsymbol{v}_0(y_1, y_2, \mu)) + A_2 a^{\alpha_2}(\boldsymbol{v}_1(\rho, \theta, \mu)) + \cdots \tag{17}$$

where $\boldsymbol{v}_i(\rho, \theta, \mu)$ is represented as:

$$\boldsymbol{v}_i(\rho, \theta, \mu) = g(\rho) \times \rho^{\alpha_i} \boldsymbol{u}^{(i)} + \hat{\boldsymbol{v}}^{(i)}(\mu) \tag{18}$$

To obtain $\hat{\boldsymbol{v}}^{(i)}(\mu)$ one has to solve the following elastic problem in the inner unbounded domain shown in Fig. 3(right).

$$\begin{aligned}
\mathcal{L}(\boldsymbol{u}^a(\mu)) &= \mathcal{L}(g(\rho)\rho^{\alpha_i}\boldsymbol{u}^{(i)}(\theta)) + \mathcal{L}(\hat{\boldsymbol{v}}^{(i)}(\mu)) = 0 \\
&\Rightarrow \mathcal{L}(\hat{\boldsymbol{v}}^{(i)}(\mu)) = 0 \quad in\ \Omega^{\mu}_{\infty} - [\rho_1 < \rho < \rho_2] \\
&\Rightarrow \mathcal{L}(\hat{\boldsymbol{v}}^{(i)}(\mu)) = -\rho^{\alpha_i}\boldsymbol{u}^{(i)}(\theta) \times \mathcal{L}\,(g(\rho)) \quad in\ [\rho_1 < \rho < \rho_2] \qquad (19) \\
\mathcal{T}(\boldsymbol{u}^a(\mu)) &= \mathcal{T}(\rho^{\alpha_1}\boldsymbol{u}^{(1)}(\theta)) + \mathcal{T}(\hat{\boldsymbol{v}}^{(i)}(\mu))) = 0 \\
&\Rightarrow \mathcal{T}(\hat{\boldsymbol{v}}^{(i)}(\mu))) = 0 \quad on\ \Gamma_1, \Gamma_2, \Gamma_5, \Gamma_6, \Gamma_7 \\
&\Rightarrow \mathcal{T}(\hat{\boldsymbol{v}}^{(i)}(\mu))) = -\rho^{\alpha_i}\boldsymbol{u}^{(i)}(\theta)\mathcal{T}(g(\rho)) \quad on\ \Gamma_3, \Gamma_4 \qquad (20)
\end{aligned}$$

On Γ_∞ we prescribe $\hat{\boldsymbol{v}}^{(i)}(\mu) \to 0$ according to (12).

2.4 Change in potential energy due to the onset of a new crack

Consider the two elastic problems in the previous two subsections, $\boldsymbol{u}^a(0)$ and $\boldsymbol{u}^a(\mu)$—the first being solved over Ω^0_{∞} and the second over Ω^{μ}_{∞}. On the boundary at $\rho \to \infty$, i.e. on Γ_∞, traction boundary conditions corresponding to the outer expansion as $r \to 0$ are considered:

$$\mathcal{T}_i(\mu)|_{\rho\to\infty} = \mathcal{T}_i(0)|_{\rho\to\infty} \stackrel{\text{def}}{=} \mathcal{T}_i|_{\rho\to\infty} \tag{21}$$

Because both $\boldsymbol{u}^a(0)$ and $\boldsymbol{u}^a(\mu)$ satisfy the equilibrium equations with no body forces (note that only $\hat{\boldsymbol{v}}^{(i)}$ are solutions to a problem with body forces but not $\boldsymbol{u}^a$) then the potential energy

of each of the two problems is:

$$\Pi(\boldsymbol{u}^a(\mu)) = \frac{1}{2}\int\limits_{\Omega^\mu_\infty} \sigma_{ij}(\mu)u^a_{i,j}(\mu)d\Omega - \int\limits_{\partial\Omega^\mu_\infty} \mathcal{T}_i(\mu)u^a_i(\mu)d\Gamma \tag{22}$$

$$\Pi(\boldsymbol{u}^a(0)) = \frac{1}{2}\int\limits_{\Omega^0_\infty} \sigma_{ij}(0)u^a_{i,j}(0)d\Omega - \int\limits_{\partial\Omega^0_\infty} \mathcal{T}_i(0)u^a_i(0)d\Gamma \tag{23}$$

On the boundary $\partial\Omega^0_\infty$ traction free BCs are prescribed except on Γ_∞, and because the crack faces are also traction free then the boundary $\partial\Omega^0_\infty$ is also traction free except on Γ_∞. Thus, (22)–(23) are:

$$\Pi(\boldsymbol{u}^a(\mu)) = \frac{1}{2}\int\limits_{\Omega^\mu_\infty} \sigma_{ij}(\mu)u^a_{i,j}(\mu)d\Omega - \int\limits_{\Gamma_\infty} \mathcal{T}_i|_{\rho\to\infty}u^a_i(\mu)d\Gamma \tag{24}$$

$$\Pi(\boldsymbol{u}^a(0)) = \frac{1}{2}\int\limits_{\Omega^0_\infty} \sigma_{ij}(0)u^a_{i,j}(0)d\Omega - \int\limits_{\Gamma_\infty} \mathcal{T}_i|_{\rho\to\infty}u^a_i(0)d\Gamma \tag{25}$$

Because Ω^μ_∞ is identical to Ω^0_∞ (they differ by a line crack only) we may subtract (23) from (22) to obtain:

$$\begin{aligned}\Pi(\boldsymbol{u}^a(\mu)) - \Pi(\boldsymbol{u}^a(0)) = \frac{1}{2}\int\limits_{\Omega^0_\infty} \left(\sigma_{ij}(\mu)u^a_{i,j}(\mu) - \sigma_{ij}(0)u^a_{i,j}(0)\right)d\Omega \\ - \int\limits_{\Gamma_\infty} \left(\mathcal{T}_i|_{\rho\to\infty}u^a_i(\mu) - \mathcal{T}_i|_{\rho\to\infty}u^a_i(0)\right)d\Gamma\end{aligned} \tag{26}$$

The area integral involving stresses times displacement derivatives is equal to the surface integral on its boundaries of tractions times displacements (see e.g. the weak form in Szabó and Babuška 1991), and since traction free boundary conditions are applied on the entire boundary except of Γ_∞, then:

$$\frac{1}{2}\int\limits_{\Omega^0_\infty} \left(\sigma_{ij}(\mu)u^a_{i,j}(\mu) - \sigma_{ij}(0)u^a_{i,j}(0)\right)d\Omega = \frac{1}{2}\int\limits_{\Gamma_\infty} \left(\mathcal{T}_i|_{\rho\to\infty}u^a_i(\mu) - \mathcal{T}_i|_{\rho\to\infty}u^a_i(0)\right)d\Gamma \tag{27}$$

Substituting (27) into (26) one obtains:

$$\begin{aligned}\delta\Pi = \Pi(\mu) - \Pi(0) &\overset{\text{def}}{=} \Pi(\boldsymbol{u}^a(\mu)) - \Pi(\boldsymbol{u}^a(0)) \\ &= -\frac{1}{2}\int\limits_{\Gamma_\infty} \left(\mathcal{T}_i|_{\rho\to\infty}u^a_i(\mu) - \mathcal{T}_i|_{\rho\to\infty}u^a_i(0)\right)d\Gamma\end{aligned} \tag{28}$$

In view of (21) we replace the first $\mathcal{T}_i|_{\rho\to\infty}$ by $\mathcal{T}_i(0)$ and the second by $\mathcal{T}_i(\mu)$ to finally obtain:

$$\delta\Pi = \Pi(\mu) - \Pi(0) \overset{\text{def}}{=} \Psi(\boldsymbol{u}^a(\mu), \boldsymbol{u}^a(0)) = \frac{1}{2}\int\limits_{\Gamma_\infty} \left(\mathcal{T}_i(\mu)u^a_i(0) - \mathcal{T}_i(0)u^a_i(\mu)\right)d\Gamma \tag{29}$$

3 Formulation of the mixed mode expression for $\delta\Pi$

The displacements for the inner expansions in the vicinity of the cracked and uncracked rounded notch tip are:

$$\begin{aligned} \boldsymbol{u}^a(\mu) &= \boldsymbol{u}_0(\mu) + A_1 a^{\alpha_1}(g(\rho)\rho^{\alpha_1}\underline{u}^{(1)}(\theta) + \hat{\boldsymbol{v}}^{(1)}(\mu)) \\ &\quad + A_2 a^{\alpha_2}(g(\rho)\rho^{\alpha_2}\boldsymbol{u}^{(2)}(\theta) + \hat{\boldsymbol{v}}^{(2)}(\mu)) + h.o.t. \qquad (30) \\ \boldsymbol{u}^a(0) &= \boldsymbol{u}_0(0) + A_1 a^{\alpha_1}(g(\rho)\rho^{\alpha_1}\boldsymbol{u}^{(1)}(\theta) + \hat{\boldsymbol{v}}^{(1)}(0)) \\ &\quad + A_2 a^{\alpha_2}(g(\rho)\rho^{\alpha_2}\boldsymbol{u}^{(2)}(\theta) + \hat{\boldsymbol{v}}^{(2)}(0)) + h.o.t. \qquad (31) \end{aligned}$$

Inserting these expressions in (29) and using the linearity property of the functional Ψ, we may compute the change in potential energy between the cracked and un-cracked states:

$$\begin{aligned} \Psi(\boldsymbol{u}^a(\mu), \boldsymbol{u}^a(0)) &= \Psi(\boldsymbol{u}_0(\mu), \boldsymbol{u}_0(0)) && (32) \\ &\quad + \Psi(\boldsymbol{u}_0(\mu), A_1 a^{\alpha_1} g(\rho)\rho^{\alpha_1}\boldsymbol{u}^{(1)}(\theta)) && (33) \\ &\quad + \Psi(\boldsymbol{u}_0(\mu), A_1 a^{\alpha_1}\hat{\boldsymbol{v}}^{(1)}(0)) && (34) \\ &\quad + \Psi(\boldsymbol{u}_0(\mu), A_2 a^{\alpha_2} g(\rho)\rho^{\alpha_2}\boldsymbol{u}^{(2)}(\theta)) && (35) \\ &\quad + v\Psi(\boldsymbol{u}_0(\mu), A_2 a^{\alpha_2}\hat{\boldsymbol{v}}^{(2)}(0)) && (36) \\ &\quad + \Psi(A_1 a^{\alpha_1}(g(\rho)\rho^{\alpha_1}\boldsymbol{u}^{(1)}(\theta), \boldsymbol{u}_0(0)) && (37) \\ &\quad + \Psi(A_1 a^{\alpha_1}(g(\rho)\rho^{\alpha_1}\boldsymbol{u}^{(1)}(\theta), A_1 a^{\alpha_1} g(\rho)\rho^{\alpha_1}\boldsymbol{u}^{(1)}(\theta)) && (38) \\ &\quad + \Psi(A_1 a^{\alpha_1}(g(\rho)\rho^{\alpha_1}\boldsymbol{u}^{(1)}(\theta), A_1 a^{\alpha_1}\hat{\boldsymbol{v}}^{(1)}(0)) && (39) \\ &\quad + \Psi(A_1 a^{\alpha_1}(g(\rho)\rho^{\alpha_1}\boldsymbol{u}^{(1)}(\theta), A_2 a^{\alpha_2} g(\rho)\rho^{\alpha_2}\boldsymbol{u}^{(2)}(\theta)) && (40) \\ &\quad + \Psi(A_1 a^{\alpha_1}(g(\rho)\rho^{\alpha_1}\boldsymbol{u}^{(1)}(\theta), A_2 a^{\alpha_2}\hat{\boldsymbol{v}}^{(2)}(0)) && (41) \\ &\quad + \Psi(A_1 a^{\alpha_1}\hat{\boldsymbol{v}}^{(1)}(\mu)), \boldsymbol{u}_0(0)) && (42) \\ &\quad + \Psi(A_1 a^{\alpha_1}\hat{\boldsymbol{v}}^{(1)}(\mu)), A_1 a^{\alpha_1} g(\rho)\rho^{\alpha_1}\boldsymbol{u}^{(1)}(\theta)) && (43) \\ &\quad + \Psi(A_1 a^{\alpha_1}\hat{\boldsymbol{v}}^{(1)}(\mu)), A_1 a^{\alpha_1}\hat{\boldsymbol{v}}^{(1)}(0)) && (44) \\ &\quad + \Psi(A_1 a^{\alpha_1}\hat{\boldsymbol{v}}^{(1)}(\mu)), A_2 a^{\alpha_2} g(\rho)\rho^{\alpha_2}\boldsymbol{u}^{(2)}(\theta)) && (45) \\ &\quad + \Psi(A_1 a^{\alpha_1}\hat{\boldsymbol{v}}^{(1)}(\mu)), A_2 a^{\alpha_2}\hat{\boldsymbol{v}}^{(2)}(0)) && (46) \\ &\quad + \Psi(A_2 a^{\alpha_2} g(\rho)\rho^{\alpha_2}\boldsymbol{u}^{(2)}(\theta), \boldsymbol{u}_0(0)) && (47) \\ &\quad + \Psi(A_2 a^{\alpha_2} g(\rho)\rho^{\alpha_2}\boldsymbol{u}^{(2)}(\theta), A_1 a^{\alpha_1} g(\rho)\rho^{\alpha_1}\boldsymbol{u}^{(1)}(\theta)) && (48) \\ &\quad + \Psi(A_2 a^{\alpha_2} g(\rho)\rho^{\alpha_2}\boldsymbol{u}^{(2)}(\theta), A_1 a^{\alpha_1}\hat{\boldsymbol{v}}^{(1)}(0)) && (49) \\ &\quad + \Psi(A_2 a^{\alpha_2} g(\rho)\rho^{\alpha_2}\boldsymbol{u}^{(2)}(\theta), A_2 a^{\alpha_2} g(\rho)\rho^{\alpha_2}\boldsymbol{u}^{(2)}(\theta)) && (50) \\ &\quad + \Psi(A_2 a^{\alpha_2} g(\rho)\rho^{\alpha_2}\boldsymbol{u}^{(2)}(\theta), A_2 a^{\alpha_2}\hat{\boldsymbol{v}}^{(2)}(0)) && (51) \\ &\quad + \Psi(A_2 a^{\alpha_2}\hat{\boldsymbol{v}}^{(2)}(\mu), \boldsymbol{u}_0(0)) && (52) \\ &\quad + \Psi(A_2 a^{\alpha_2}\hat{\boldsymbol{v}}^{(2)}(\mu), A_1 a^{\alpha_1} g(\rho)\rho^{\alpha_1}\boldsymbol{u}^{(1)}(\theta)) && (53) \\ &\quad + \Psi(A_2 a^{\alpha_2}\hat{\boldsymbol{v}}^{(2)}(\mu), A_1 a^{\alpha_1}\hat{\boldsymbol{v}}^{(1)}(0)) && (54) \\ &\quad + \Psi(A_2 a^{\alpha_2}\hat{\boldsymbol{v}}^{(2)}(\mu), A_2 a^{\alpha_2} g(\rho)\rho^{\alpha_2}\boldsymbol{u}^{(2)}(\theta)) && (55) \\ &\quad + \Psi(A_2 a^{\alpha_2}\hat{\boldsymbol{v}}^{(2)}(\mu), A_2 a^{\alpha_2}\hat{\boldsymbol{v}}^{(2)}(0)) && (56) \end{aligned}$$

The lengthy expression above may be simplified as follows. Because $\Psi(f, f) = 0$, the integrals (38) and (50) vanish. Expression (33) which contains only the rigid body displacements is also zero. Because the boundary conditions on the inner domain dictate that

$\mathcal{T}(\hat{\boldsymbol{v}}^{(i)}(\mu)) = -\mathcal{T}(g(\rho)\rho^{\alpha_i}\boldsymbol{u}^{(i)}(\theta))$ we obtain that the following paired terms (33) (34), (35) (36), (37) (42), (47) (52) cancel each other. Terms (38), (45), (46) added together result in:

$$
\begin{aligned}
&= \frac{A_1^2 a^{2\alpha_1}}{2}\left(\int (\mathcal{T}(g(\rho)\rho^{\alpha_1}\boldsymbol{u}^{(1)}(\theta))\hat{\boldsymbol{v}}^{(1)}(0)d\Gamma - \int \mathcal{T}(\hat{\boldsymbol{v}}^{(1)}(0))g(\rho)\rho^{\alpha_1}\boldsymbol{u}^{(1)}(\theta))d\Gamma\right.\\
&\quad + \int (\mathcal{T}(\hat{\boldsymbol{v}}^{(1)}(\mu))\hat{\boldsymbol{v}}^{(1)}(0)d\Gamma - \int \mathcal{T}(\hat{\boldsymbol{v}}^{(1)}(0))\hat{\boldsymbol{v}}^{(1)}(\mu))d\Gamma\\
&\quad \left. + \int (\mathcal{T}(\hat{\boldsymbol{v}}^{(1)}(\mu))g(\rho)\rho^{\alpha_1}\boldsymbol{u}^{(1)}(\theta)d\Gamma - \int \mathcal{T}(g(\rho)\rho^{\alpha_1}\boldsymbol{u}^{(1)}(\theta))\hat{\boldsymbol{v}}^{(1)}(\mu))d\Gamma\right)
\end{aligned}
$$

The above expression corresponds to mode I loading. Terms (51), (55), (56) added together result in:

$$
\begin{aligned}
&= \frac{A_2^2 a^{2\alpha_2}}{2}\left(\int (\mathcal{T}(g(\rho)\rho^{\alpha_2}\boldsymbol{u}^{(2)}(\theta))\hat{\boldsymbol{v}}^{(2)}(0)d\Gamma - \int \mathcal{T}(\hat{\boldsymbol{v}}^{(2)}(0))g(\rho)\rho^{\alpha_2}\boldsymbol{u}^{(2)}(\theta))d\Gamma\right.\\
&\quad + \int (\mathcal{T}(\hat{\boldsymbol{v}}^{(2)}(\mu))\hat{\boldsymbol{v}}^{(2)}(0)d\Gamma - \int \mathcal{T}(\hat{\boldsymbol{v}}^{(2)}(0))\hat{\boldsymbol{v}}^{(2)}(\mu))d\Gamma\\
&\quad \left. + \int (\mathcal{T}(\hat{\boldsymbol{v}}^{(2)}(\mu))g(\rho)\rho^{\alpha_2}\boldsymbol{u}^{(2)}(\theta)d\Gamma - \int \mathcal{T}(g(\rho)\rho^{\alpha_2}\boldsymbol{u}^{(2)}(\theta))\hat{\boldsymbol{v}}^{(2)}(\mu))d\Gamma\right)
\end{aligned}
$$

This expression corresponds to mode II loading. The remaining terms are mixed mode terms which yield:

$$
\begin{aligned}
&= \frac{A_1 A_2 a^{\alpha_1+\alpha_2}}{2}\left(\int (\mathcal{T}(g(\rho)\rho^{\alpha_1}\boldsymbol{u}^{(1)}(\theta))\hat{\boldsymbol{v}}^{(2)}(0)d\Gamma\right.\\
&\quad - \int \mathcal{T}(\hat{\boldsymbol{v}}^{(2)}(0))g(\rho)\rho^{\alpha_1}\boldsymbol{u}^{(1)}(\theta))d\Gamma\\
&\quad + \int (\mathcal{T}(\hat{\boldsymbol{v}}^{(1)}(\mu))g(\rho)\rho^{\alpha_2}\boldsymbol{u}^{(2)}(\theta)d\Gamma - \int \mathcal{T}(g(\rho)\rho^{\alpha_2}\boldsymbol{u}^{(2)}(\theta))\hat{\boldsymbol{v}}^{(1)}(\mu))d\Gamma\\
&\quad + \int (\mathcal{T}(\hat{\boldsymbol{v}}^{(1)}(\mu))\hat{\boldsymbol{v}}^{(2)}(0)d\Gamma - \int \mathcal{T}(\hat{\boldsymbol{v}}^{(2)}(0))\hat{\boldsymbol{v}}^{(1)}(\mu))d\Gamma\\
&\quad + \int (\mathcal{T}(g(\rho)\rho^{\alpha_2}\boldsymbol{u}^{(2)}(\theta))\hat{\boldsymbol{v}}^{(1)}(0)d\Gamma - \int \mathcal{T}(\hat{\boldsymbol{v}}^{(1)}(0))g(\rho)\rho^{\alpha_2}\boldsymbol{u}^{(2)}(\theta))d\Gamma\\
&\quad + \int (\mathcal{T}(\hat{\boldsymbol{v}}^{(2)}(\mu))g(\rho)\rho^{\alpha_1}\boldsymbol{u}^{(1)}(\theta)d\Gamma - \int \mathcal{T}(g(\rho)\rho^{\alpha_1}\boldsymbol{u}^{(1)}(\theta))\hat{\boldsymbol{v}}^{(2)}(\mu))d\Gamma\\
&\quad \left. + \int (\mathcal{T}(\hat{\boldsymbol{v}}^{(2)}(\mu))\hat{\boldsymbol{v}}^{(1)}(0)d\Gamma - \int \mathcal{T}(\hat{\boldsymbol{v}}^{(1)}(0))\hat{\boldsymbol{v}}^{(2)}(\mu))d\Gamma\right)
\end{aligned}
$$

Taking into consideration the following properties:

(1) $\hat{\boldsymbol{v}}^{(i)}(\mu) = \hat{\boldsymbol{v}}^{(i)}(0) = 0$ on the outer boundary Γ_∞.
(2) The rounding and crack edges as well as the notch edges except Γ_3, Γ_4 are traction free therefore $\mathcal{T}(\hat{\boldsymbol{v}}^{(i)}(\mu)) = \mathcal{T}(\hat{\boldsymbol{v}}^{(i)}(0)) = 0$ on Γ_1, Γ_2, Γ_5, Γ_6, Γ_7.
(3) On Γ_6, Γ_7 $\mathcal{T}(\hat{\boldsymbol{v}}^{(i)}(\mu)) = -\mathcal{T}(g(\rho)\rho^{\alpha_i}\boldsymbol{u}^{(i)}(\theta))$,

the integral on Γ_∞ is the only one that does not vanish:

$$\begin{aligned}\delta\Pi = &\frac{A_1^2 a^{2\alpha_1}}{2}\left(\int_{\Gamma_\infty}(\mathcal{T}(\hat{\boldsymbol{v}}^{(1)}(\mu))\rho^{\alpha_1}\boldsymbol{u}^{(1)}(\theta)d\Gamma - \int_{\Gamma_\infty}\mathcal{T}(\hat{\boldsymbol{v}}^{(1)}(0))\rho^{\alpha_1}\boldsymbol{u}^{(1)}(\theta))d\Gamma\right)\\ &+\frac{A_1 A_2 a^{\alpha_1+\alpha_2}}{2}\left(\int_{\Gamma_\infty}(\mathcal{T}(\hat{\boldsymbol{v}}^{(1)}(\mu))\rho^{\alpha_2}\boldsymbol{u}^{(2)}(\theta)d\Gamma + \int_{\Gamma_\infty}\mathcal{T}(\hat{\boldsymbol{v}}^{(2)}(\mu))\rho^{\alpha_1}\boldsymbol{u}^{(1)}(\theta))d\Gamma\right.\\ &\left.-\int_{\Gamma_\infty}(\mathcal{T}(\hat{\boldsymbol{v}}^{(1)}(0))\rho^{\alpha_2}\boldsymbol{u}^{(2)}(\theta)d\Gamma - \int_{\Gamma_\infty}\mathcal{T}(\hat{\boldsymbol{v}}^{(2)}(0))\rho^{\alpha_1}\boldsymbol{u}^{(1)}(\theta))d\Gamma\right)\\ &+\frac{A_2^2 a^{2\alpha_2}}{2}\left(\int_{\Gamma_\infty}(\mathcal{T}(\hat{\boldsymbol{v}}^{(2)}(\mu))\rho^{\alpha_1}\boldsymbol{u}^{(2)}(\theta)d\Gamma - \int_{\Gamma_\infty}\mathcal{T}(\hat{\boldsymbol{v}}^{(2)}(0))\rho^{\alpha_1}\boldsymbol{u}^{(2)}(\theta))d\Gamma\right)\end{aligned}$$

Defining the functions:

$$\begin{aligned}H_{ij}(\mu,\theta) &= -\Psi(\hat{\boldsymbol{v}}^{(i)}(\mu)),\rho^{\alpha_j}\boldsymbol{u}^{(j)}(\theta))\\ &\stackrel{\text{def}}{=} -\frac{1}{2}\int_{\Gamma_\infty}\left(\mathcal{T}(\hat{\boldsymbol{v}}^{(i)}(\mu)))\rho^{\alpha_j}\boldsymbol{u}^{(j)}(\theta) - \mathcal{T}(\rho^{\alpha_j}\boldsymbol{u}^{(j)}(\theta))\hat{\boldsymbol{v}}^{(i)}(\mu))\right)d\Gamma,\end{aligned}$$

and because $\hat{\boldsymbol{v}}^{(i)} = 0$ on Γ_∞, the above expression reduces to:

$$H_{ij}(\mu,\theta) = -\Psi(\hat{\boldsymbol{v}}^{(i)}(\mu)),\rho^{\alpha_j}\boldsymbol{u}^{(j)}(\theta)) \stackrel{\text{def}}{=} -\frac{1}{2}\int_{\Gamma_\infty}\mathcal{T}(\hat{\boldsymbol{v}}^{(i)}(\mu)))\rho^{\alpha_j}\boldsymbol{u}^{(j)}(\theta)d\Gamma,$$

and specifically:

$$\begin{aligned}H_{11}(\mu,\theta) &= -\frac{1}{2}\int_{\Gamma_\infty}(\mathcal{T}(\hat{\boldsymbol{v}}^{(1)}(\mu))\rho^{\alpha_1}\boldsymbol{u}^{(1)}(\theta)d\Gamma \qquad (57)\\ H_{11}(0) &= -\frac{1}{2}\int_{\Gamma_\infty}\mathcal{T}(\hat{\boldsymbol{v}}^{(1)}(0))\rho^{\alpha_1}\boldsymbol{u}^{(1)}(\theta))d\Gamma\\ H_{12}(\mu,\theta) &= -\frac{1}{2}\int_{\Gamma_\infty}(\mathcal{T}(\hat{\boldsymbol{v}}^{(1)}(\mu))\rho^{\alpha_2}\boldsymbol{u}^{(2)}(\theta)d\Gamma\\ H_{21}(\mu,\theta) &= -\frac{1}{2}\int_{\Gamma_\infty}(\mathcal{T}(\hat{\boldsymbol{v}}^{(2)}(\mu))\rho^{\alpha_1}\boldsymbol{u}^{(1)}(\theta)d\Gamma\\ H_{12}(0) &= -\frac{1}{2}\int_{\Gamma_\infty}(\mathcal{T}(\hat{\boldsymbol{v}}^{(1)}(0))\rho^{\alpha_2}\boldsymbol{u}^{(2)}(\theta)d\Gamma\end{aligned}$$

$$H_{21}(0) = -\frac{1}{2}\int_{\Gamma_\infty} (\mathcal{T}(\hat{\boldsymbol{v}}^{(2)}(0)))\rho^{\alpha_1}\boldsymbol{u}^{(1)}(\theta)d\Gamma$$
$$H_{22}(\mu,\theta) = -\frac{1}{2}\int_{\Gamma_\infty} (\mathcal{T}(\hat{\boldsymbol{v}}^{(2)}(\mu))\rho^{\alpha_2}\boldsymbol{u}^{(2)}(\theta)d\Gamma$$
$$H_{22}(0) = -\frac{1}{2}\int_{\Gamma_\infty} \mathcal{T}(\hat{\boldsymbol{v}}^{(2)}(0))\rho^{\alpha_2}\boldsymbol{u}^{(2)}(\theta))d\Gamma$$

Remark 3 Notice that H_{ij} are also functions of the opening angle ω.

The change in potential energy may be more compactly represented as:

$$\begin{aligned}-\delta\Pi = {} & A_1^2 a^{2\alpha_1}(H_{11}(\mu,\theta) - H_{11}(0)) \\ & + A_1 A_2 a^{\alpha_1+\alpha_2}((H_{12}(\mu,\theta) + H_{21}(\mu,\theta)) - (H_{12}(0) + H_{21}(0))) \\ & + A_2^2 a^{2\alpha_2}(H_{22}(\mu,\theta) - H_{22}(0))\end{aligned} \tag{58}$$

With the additional definition:

$$\begin{aligned}\Delta H_{11}(\mu,\theta) &= H_{11}(\mu,\theta) - H_{11}(0) \\ \Delta H_{1221}(\mu,\theta) &= (H_{12}(\mu,\theta) + H_{21}(\mu,\theta)) - (H_{12}(0) + H_{21}(0)) \\ \Delta H_{22}(\mu,\theta) &= H_{22}(\mu,\theta) - H_{22}(0)\end{aligned}$$

Equation 58 takes the form:

$$-\delta\Pi = A_1^2 a^{2\alpha_1}(\Delta H_{11}(\mu,\theta) + m\Delta H_{1221}(\mu,\theta) + m^2\Delta H_{22}(\mu,\theta)) \tag{59}$$

where $m = \frac{A_2}{A_1}a^{\alpha_2-\alpha_1}$ is the mixity ratio.

Remark 4 Given ΔH_{ij} for E and ν, one may easily obtain ΔH_{ij} for any E_{new} and ν_{new} by the following connection:

$$\Delta H_{ij}^{new}(\omega,\theta_0) = \Delta H_{ij}(\omega,\theta_0)\frac{E}{1-\nu^2}\frac{1-\nu_{new}^2}{E_{new}} \tag{60}$$

Remark 5 For mode I loading we defined $h(\mu)$ (Leguillon and Yosibash 2003) as follows:

$$h(\mu) = \frac{H_{11}(\mu) - H_{11}(0)}{\bar{H}_{11}\mu^{2\alpha_1}} \tag{61}$$

were $h(\mu)$ is a function which is independent of the elastic properties of the material and tends toward 1 as $\mu \to \infty$ and $\bar{H}_{11}$ is the value of $H_{11}(\mu)$ when $a \to 0$ i.e. the sharp V-notch case.

4 The failure criterion

Using (59) the energy criterion reads:

$$\frac{-\delta\Pi}{\ell} \geq G_c, \;\Rightarrow\; \ell G_c \leq A_1^2 a^{2\alpha_1}\left(\Delta H_{11}(\mu,\theta) + m\Delta H_{1221}(\mu,\theta) + m^2\Delta H_{22}(\mu,\theta)\right) \tag{62}$$

Multiply and divide (62) by $\bar{H}_{11}(\theta)+\bar{m}(\bar{H}_{12}(\theta)+\bar{H}_{21}(\theta))+\bar{m}^2\bar{H}_{22}(\theta)$ where $\bar{H}_{ij}(\theta)$ and $\bar{m}=\frac{A_2}{A_1}\tilde{\ell}^{\alpha_2-\alpha_1}$ are associated with the sharp V-notch case (Yosibash et al. 2006). Since $a=\frac{\ell}{\mu}$ we may write:

$$G_c \le A_1^2 \ell^{2\alpha_1-1}\left(\bar{H}_{11}(\theta)+\bar{m}(\bar{H}_{12}(\theta)+\bar{H}_{21}(\theta))+\bar{m}^2\bar{H}_{22}(\theta)\right)\times h^{mixed}(\mu) \tag{63}$$

where $h^{mixed}(\mu)$ is defined:

$$h^{mixed}(\mu,\theta)\overset{\text{def}}{=}\frac{\Delta H_{11}(\mu,\theta)+m\Delta H_{1221}(\mu,\theta)+m^2\Delta H_{22}(\mu,\theta)}{(\bar{H}_{11}(\theta)+\bar{m}(\bar{H}_{12}(\theta)+\bar{H}_{21}(\theta))+\bar{m}^2\bar{H}_{22}(\theta))\cdot\mu^{2\alpha_1}} \tag{64}$$

The stress criterion requires that along a distance ℓ measured from the rounded tip at an angle θ the normal stress has to exceed the material critical stress σ_c.

$$\begin{aligned}\boldsymbol{\sigma}_n(\boldsymbol{u}^a(0,\ell,0)) = {} & A_1 a^{\alpha_1-1}\boldsymbol{\sigma}_n(g(\rho)\rho^{\alpha_1}\underline{u}^{(1)}(\theta)+\hat{\boldsymbol{v}}^{(1)}(0)) \\ & + A_2 a^{\alpha_2-1}\boldsymbol{\sigma}_n(g(\rho)\rho^{\alpha_2}\underline{u}^{(2)}(\theta)+\hat{\boldsymbol{v}}^{(2)}(0)) \ge \sigma_c\end{aligned} \tag{65}$$

Because it is assumed that ℓ is small and in the vicinity of the rounding $g(\rho)=0$ one obtains:

$$\boldsymbol{\sigma}_n(\boldsymbol{u}^a(0,l,0)) = A_1 a^{\alpha_1-1}(\boldsymbol{\sigma}_n(\hat{\boldsymbol{v}}^{(1)}(0))+m\boldsymbol{\sigma}_n(\hat{\boldsymbol{v}}^{(2)}(0)) \ge \sigma_c. \tag{66}$$

$\boldsymbol{\sigma}_n(\boldsymbol{u}^a(0,\ell,0))$ is a decreasing function of ℓ and $\delta\Pi$ is an increasing function of ℓ. For a specific ℓ_0 the two criteria coincide with their material critical values σ_c and G_c.

For that ℓ_0 both (64) and (66) inequalities become equal, so dividing (64) by the square of (66) one obtains:

$$\ell_0\frac{(\bar{H}_{11}(\theta)+\bar{m}(\bar{H}_{12}(\theta)+\bar{H}_{21}(\theta))+\bar{m}^2\bar{H}_{22}(\theta))(h_{mixed}(\mu_0,\theta))\cdot\mu_0^{2\alpha-2}}{(\boldsymbol{\sigma}_n(\hat{\boldsymbol{v}}^{(1)}(0))+m\boldsymbol{\sigma}_n(\hat{\boldsymbol{v}}^{(2)}(0))^2}=\frac{G_c}{\sigma_c^2} \tag{67}$$

where $\mu_0=\ell_0/a$. Defining $H^{mixed}(\mu)$:

$$H^{mixed}(\mu,\theta)\overset{\text{def}}{=}\frac{h^{mixed}(\mu,\theta)\cdot\mu^{2\alpha_1-1}}{(\boldsymbol{\sigma}_n(\hat{\boldsymbol{v}}^{(1)}(0))+m\boldsymbol{\sigma}_n(\hat{\boldsymbol{v}}^{(2)}(0))^2} \tag{68}$$

Equation 67 becomes:

$$a\left(\bar{H}_{11}(\theta)+\bar{m}(\bar{H}_{12}(\theta)+\bar{H}_{21}(\theta))+\bar{m}^2\bar{H}_{22}(\theta)\right)H^{mixed}(\mu_0,\theta)=\frac{G_c}{\sigma_c^2} \tag{69}$$

The function $H^{mixed}(\mu,\theta)$ is independent of the elastic properties of the material.

As an example, $H^{mixed}(\mu,\theta^*)$ is computed for different m's for $a=0.03\,\text{mm}$ and $\omega=315^\circ$ and plotted in Fig. 4.

For an assumed sharp V-notch, the mode mixity ratio $\bar{m}$ can be computed as well as the $\bar{H}_{ij}$ values (Yosibash et al. 2006). Then for a rounded V-notch, with a given notch radius a, the value of m is determined and (69) provides $H^{mixed}(\mu,\theta^*)$ for any μ and θ^*. From plots such as 4 for a given θ_i one can obtain μ_o therefore ℓ_0. Once ℓ_0 is obtained it can be inserted back into (62) and a critical mode I GSIF is obtained:

$$A_{1c}^{blunt}=\sqrt{\frac{G_c\ell_0}{a^{2\alpha_1}(\Delta H_{11}(\mu_0,\theta^*)+m\Delta H_{1221}(\mu_0,\theta^*)+m^2\Delta H_{22}(\mu_0,\theta^*))}} \tag{70}$$

The crack initiation angle is the angle at which the minimum value of A_{1c}^{blunt} is obtained. Numerical investigations show that the crack initiation angle θ_i for a sharp V-notch is similar to the blunt V-notch therefore being used for the blunt V-notch.

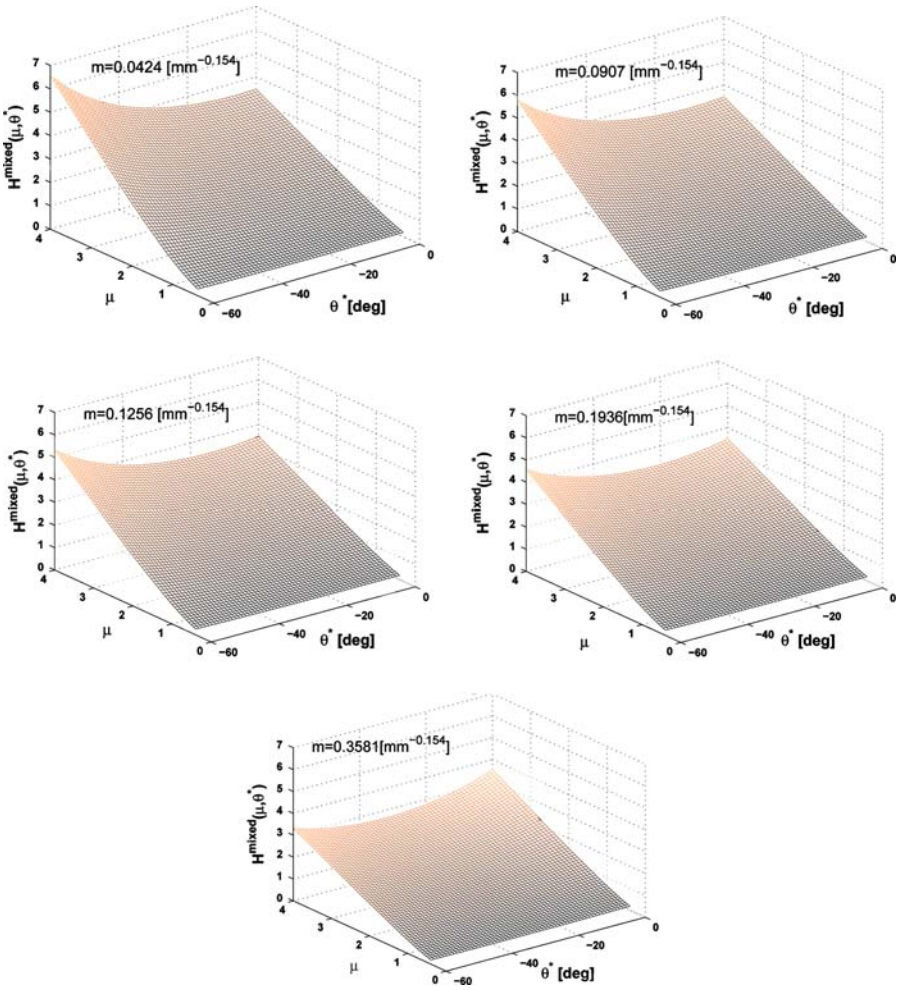

Fig. 4 $H^{mixed}(\mu, \theta^*)$ for $m = 00424, 00907, 01256, 01936, 03581$ for $a = 0.03$ mm and $\omega = 315°$

4.1 Retrieving the sharp V-notch criterion as $a \to 0$

The blunt notch criterion must tend to the sharp notch criterion as $a \to 0$ (i.e. $\mu \to \infty$). The function $h^{mixed}(\mu, \theta^*)$ (independent of the elastic properties of the material) is an increasing function of μ and for a given θ_i tends toward 1 as $\mu \to \infty$. As an example $h^{mixed}(\mu, \theta^*)$ for a PMMA specimen with $E = 3100\,\text{MPa}$, $\nu = 0.36$, $K_{Ic} = 1.12\,\text{MPa}\sqrt{m}$ and $\frac{A_2}{A_1} = 0.216$ is plotted in Fig. 5. The predicted crack initiation angle using the sharp criterion presented in Yosibash et al. (2006) is $\theta_i^* \approx -18°$. Figure 5 demonstrates that $h^{mixed}(\mu, \theta_i^* = -18°)$ tends toward 1 as $a \to 0$ ($\mu \to \infty$).

Consider next $H^{mixed}(\mu, \theta^*)$ in (68). As $a \to 0$ then by definition $m \to 0$ and the expression $(\boldsymbol{\sigma}_n(\hat{\boldsymbol{v}}^{(1)}(0)) + m\boldsymbol{\sigma}_n(\hat{\boldsymbol{v}}^{(2)}(0)) \to \boldsymbol{\sigma}_n(\hat{\boldsymbol{v}}^{(1)}(0))$. Also notice that $\boldsymbol{\sigma}_n(\hat{\boldsymbol{v}}^{(1)}(0))$ for $\mu \to \infty$ decreases to zero according the to first eigen-function thus $\boldsymbol{\sigma}_n(\hat{\boldsymbol{v}}^{(1)}(0)) \to \mu^{\alpha_1 - 1}$. Notice that as $\mu \to \infty$, $h^{mixed}(\mu, \theta_i^*) \to 1$ then, according to (68)

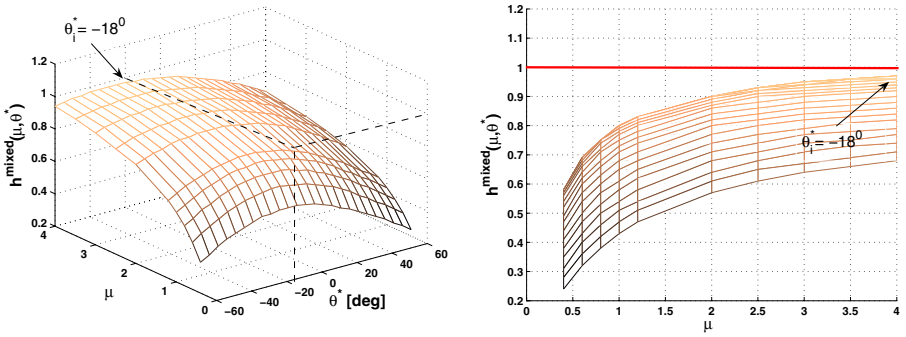

Fig. 5 $h^{mixed}(\mu, \theta_i)$ for PMMA having a V-notch angle $\omega = 315°$ ($E = 3100\,\text{MPa}$, $\nu = 0.36$, $K_{Ic} = 1.12\,\text{MPa}\sqrt{m}$)

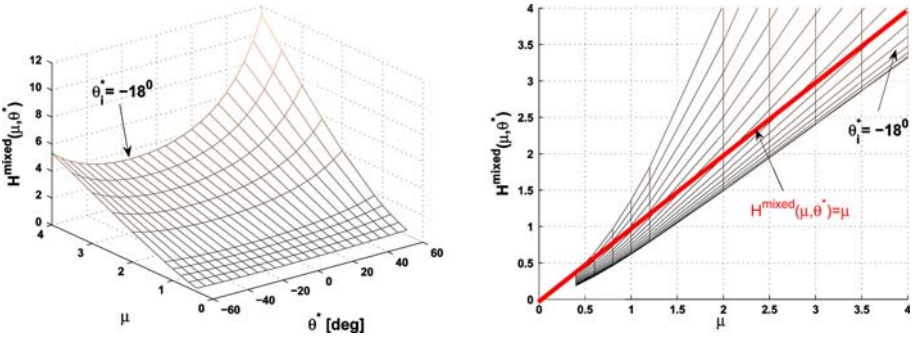

Fig. 6 $H^{mixed}(\mu, \theta_i^*)$ tending toward μ as $a \to 0$

$H^{mixed}(\mu, \theta_i) \to \mu$—this can be also noticed in Fig. 6. For $H^{mixed}(\mu, \theta_i) \to \mu$ (69) reduces to the known sharp notch failure criterion presented in Yosibash et al. (2006).

5 Numerical results

This section summarizes the various entities required for the application of the failure criterion after being computed by finite element methods.

5.1 Mode I loading alone: computing $\hat{\boldsymbol{v}}^{(1)}(0)$, $\hat{\boldsymbol{v}}^{(1)}(\mu)$, ΔH_{11}, and $h(\mu)$

To compute the $\hat{\boldsymbol{v}}^{(1)}$ function we generated a p-FE model representing the unbounded domain. Since we need to compute both $\hat{\boldsymbol{v}}^1(0)$ and $\hat{\boldsymbol{v}}^1(\mu)$ we have two unbounded domains. One domain represents the un-cracked blunt notch and the second represents the cracked blunt notch (see Fig. 7).

In practice we used an outer domain of radius $\rho_\infty = 250$ and checked that the results are virtually unchanged when ρ_∞ was increased to $\rho_\infty = 500$.

We also investigated the influence of the cutoff function boundaries by performing computations for $\rho_1 = 80$, $\rho_2 = 110$ as well as with $\rho_1 = 150$, $\rho_2 = 200$.

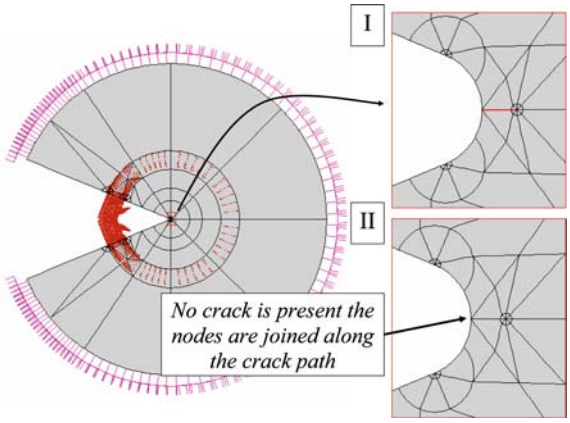

Fig. 7 FE models generated for computing the $\hat{\boldsymbol{v}}^{(i)}$ functions

Once the value of $\mathcal{T}(\hat{\boldsymbol{v}}^{(1)}(\mu))$ and $\mathcal{T}(\hat{\boldsymbol{v}}^{(1)}(0))$ are obtained by the FE analysis we may compute $\delta\Pi$.

$$\begin{aligned}\frac{-\delta\Pi}{A_1^2 a^{2\alpha_1}} &= H_{11}(\mu) - H_{11}(0)\\ &= \frac{1}{2}\int_{\Gamma_1}\{\mathcal{T}(\hat{\boldsymbol{v}}^{(1)}(\mu))\rho^{\alpha_1}\boldsymbol{u}^{(1)}(\theta)\}d\Gamma - \frac{1}{2}\int_{\Gamma_1}\{\mathcal{T}(\hat{\boldsymbol{v}}^{(1)}(0))\rho^{\alpha_1}\boldsymbol{u}^{(1)}(\theta))\}d\Gamma\\ &= \frac{1}{2}\int_{\Gamma_1}\{\sigma_{rr}^{(1)}(\hat{\boldsymbol{v}}^{(1)}(\mu))R^{\alpha_1}u_r^{(1)}(\theta) + \sigma_{r\theta}^{(1)}(\hat{\boldsymbol{v}}^{(1)}(\mu))R^{\alpha_1}u_\theta^{(1)}(\theta)\}Rd\theta\\ &\quad -\frac{1}{2}\int_{\Gamma_1}\{\sigma_{rr}^{(1)}(\hat{\boldsymbol{v}}^{(1)}(0))R^{\alpha_1}u_r^{(1)}(\theta) + \sigma_{r\theta}^{(1)}(\hat{\boldsymbol{v}}^{(1)}(0))R^{\alpha_1}u_\theta^{(1)}(\theta)\}Rd\theta \qquad (71)\end{aligned}$$

The integrals are computed numerically using a Gauss quadrature of $N = 92$ points:

$$\begin{aligned}H_{11}(\mu) &= \frac{R^{\alpha_1+1}}{2}\frac{\omega}{2}\sum_{i=1}^{N} W_i(\sigma_{rr}^{\mu}(\theta_i)u_r^{(1)}(\theta) + \sigma_{r\theta}^{\mu}(\theta_i)u_\theta^{(1)}(\theta))_{r=R}\\ H_{11}(0) &= \frac{R^{\alpha_1+1}}{2}\frac{\omega}{2}\sum_{i=1}^{N} W_i(\sigma_{rr}^{0}(\theta_i)u_r^{(1)}(\theta) + \sigma_{r\theta}^{0}(\theta_i)u_\theta^{(1)}(\theta))_{r=R} \qquad (72)\end{aligned}$$

To check that the computation of the $H_{11}(\mu)$ and $H_{11}(0)$ are correct, we also computed the potential energy for the entire domain with and without a crack, together with the generalized stress intensity factor A_1 using the FE models shown in Fig. 8.

The values of $H_{11}(\mu)$, $H_{11}(0)$ for $E = 1$, $\nu = 0.3$ and their accuracy are given for different crack lengths μ, and for 4 different V-notch opening angles for $a = 0.03$ mm in Table 2.

One may notice the excellent accuracy obtained for $\delta\Pi$ using the computed $H_{11}(\mu) - H_{11}(0)$. In Fig. 9 we plot $h(\mu)$ showing that indeed it tends to 1 as μ increases.

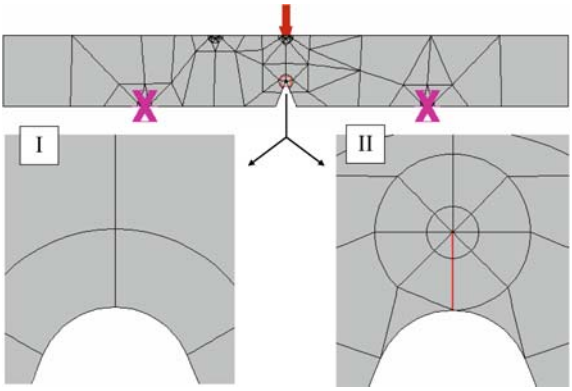

Fig. 8 FE models for computing $\delta\Pi$

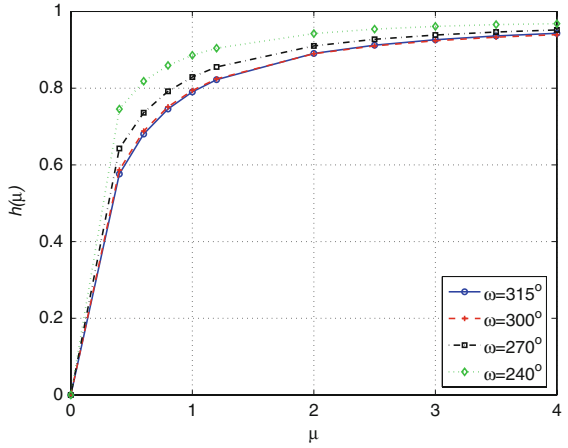

Fig. 9 $h(\mu)$ for different V-notch opening angles ($E = 1, \nu = 0.3, a = 0.03\,\text{mm}$)

5.2 Mixed mode loading: computing $\hat{\boldsymbol{v}}^{(i)}(0)$, $\hat{\boldsymbol{v}}^{(i)}(\mu)$, ΔH_{ij}, $h^{mixed}(\mu, \theta^*)$ and $H^{mixed}(\mu, \theta^*)$

Again we compute the $\hat{\boldsymbol{v}}^{(i)}$ functions by p-FE models representing the unbounded domain (see Fig. 10) with the outer radius $\rho_\infty = 250$ and $\rho_1 = 80$, $\rho_2 = 110$.

To verify the accuracy of our computations, we also computed the potential energy for the entire domain with and without a crack, together with the generalized stress intensity factors A_1, A_2 using the FE models shown in Fig. 11.

The values of $H_{ij}(\mu)$, $H_{ij}(0)$ for $E = 1$, $\nu = 0.3$ and their accuracy are given for different crack lengths μ, for the V-notch opening angle $\omega = 315°$ at various crack inclination angles for $a = 0.03\,\text{mm}$ in Tables 3 and 4.

In Fig. 12 we plot $h(\mu)$, $h^{mixed}(\mu, \theta^* = 0)$ showing that indeed it tends to 1 as μ increases.

The values of ΔH_{ij} for $\theta^* = -60 \to 60$ and $\mu = 0 \to 4$ are summarized in Table 5 and shown graphically in Fig. 13 for $\omega = 315°$. Same data for $\omega = 270°$ is provided in Table 6 and Fig. 14.

It should be noted that ΔH_{11} and ΔH_{22} are symmetric with respect to θ^* whereas ΔH_{1221} is antisymmetric. One can also notice that the trend of the various ΔH_{ij} for the blunt notch case is similar to the trend observed for the sharp notch case (see Fig. 15).

Table 2 Mode I loading: $H_{11}(\mu)$ for $E = 1$, $\nu = 0.3$, $a = 0.03$, $\rho_1 = 80$, $\rho_2 = 110$, $\rho_\infty = 250$

μ	$H_{11}(\mu)$	ΔH_{11}	$\delta\Pi^{FE}$	ΔH_{11}^{FE} (% error)	$h(\mu)$	$H_{11}(\mu)$	ΔH_{11}	$\delta\Pi^{FE}$	ΔH_{11}^{FE} (% error)	$h(\mu)$
$\omega = 315°$						$\omega = 300°$				
0	−7.8195	0	0	0 (NA)	0	−4.6665	0	0	0	0
0.4	−6.5470	1.2724	2.60E-2	1.2602 (0.97%)	0.5763	−3.4178	1.2487	2.51E-2	1.2406 (0.65%)	0.5866
0.6	−5.5572	2.2622	4.64E-2	2.2489 (0.59%)	0.6802	−2.4476	2.2189	4.48E-2	2.2127 (0.28%)	0.6881
0.8	−4.5035	3.3159	6.82E-2	3.3055 (0.31%)	0.7457	−1.4138	3.2531	6.58E-2	3.2531 (0.00%)	0.7513
1.0	−3.4176	4.4018	9.08E-2	4.3989 (0.06%)	0.7901	−0.3461	4.3204	8.76E-2	4.3311 (−0.25%)	0.7940
1.2	−2.3139	5.5055	1.14E-1	5.5151 (−0.17%)	0.8220	0.7404	5.4069	1.10E-1	5.4337 (−0.49%)	0.8243
2.0	2.1709	9.9904			0.8904	5.1823	9.8489			0.8897
2.5	5.0019	12.8214			0.9121	7.9969	12.6634			0.9102
3	7.8349	15.6543			0.9264	10.8228	15.4893			0.9236
3.5	10.6657	18.4852			0.9362	13.6543	18.3208			0.9329
4.0	13.4921	21.3116			0.9431	16.4871	21.1536			0.9394
$\omega = 270°$						$\omega = 240°$				
0	−1.0907	0	0	0 (NA)	0	−0.6359	0	0	0	0
0.4	0.0068	1.1600	2.07E-2	1.1544 (0.41%)	0.6427	0.3358	0.9716	1.25E-2	0.9626 (0.94%)	0.7454
0.6	0.9735	2.0600	3.70E-2	2.0625 (0.09%)	0.7359	1.1212	1.7571	2.26E-2	1.7485 (0.49%)	0.8181
0.8	1.9479	3.0400	5.46E-2	3.0435 (−0.16%)	0.7919	1.9946	2.6305	3.40E-2	2.6239 (0.25%)	0.8594
1.0	2.965	4.0600	7.30E-2	4.0708 (−0.36%)	0.8290	2.9333	3.5692	4.62E-2	3.5665 (0.08%)	0.8859
1.2	4.012	5.1000	9.21E-2	5.1316 (−0.57%)	0.8552	3.9246	4.5605	5.91E-2	4.5631 (−0.06%)	0.9043
2.0	8.3813	9.4720			0.9102	8.2792	8.9151			0.9424
2.5	11.2146	12.3052			0.9273	11.2417	11.8776			0.9539
3	14.1000	15.1907			0.9386	11.2417	11.8776			0.9539
3.5	17.0252	18.1158			0.9464	17.5630	18.1989			0.9657
4.0	19.9824	21.0731			0.9519	20.8689	21.5048			0.9681

$\Delta H_{11} \overset{\text{def}}{=} H_{11}(\mu) - H_{11}(0)$

$\Delta H_{11}^{FE} = \frac{-\delta\Pi^{FE}}{A_1^2 a^{2\alpha_1}}$ is the value obtained from the FE models in Fig. 8 with and without the crack

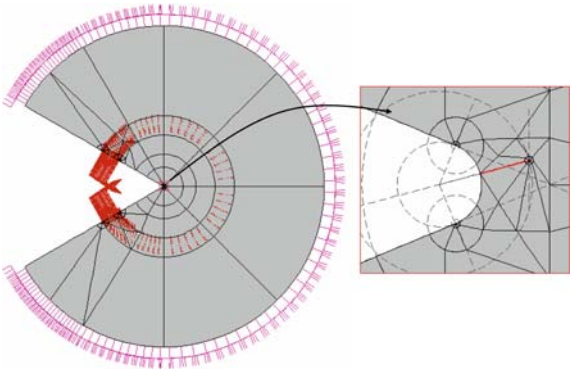

Fig. 10 FE models generated for computing the $\hat{\boldsymbol{v}}^{(i)}$ functions for the mixed mode loading

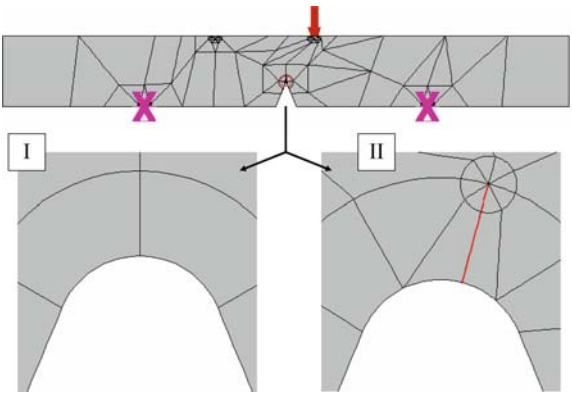

Fig. 11 FE models for computing $\delta\Pi$ under mixed mode loading

To verify that (59) provides good estimates, we computed $\delta\Pi$ using it and by direct FE analysis. Consider a 3PB specimen made of PMMA with $E = 3100\,\text{MPa}$, $\nu = 0.36$ containing a blunt notch $a = 0.03\,\text{mm}$ as shown in Fig. 11. We constructed a FE model of the specimen with and without a finite crack $\ell = 0.036\,\text{mm}$, $\theta^* = -10^\circ$ at the blunt notch tip. We loaded the FE models with an arbitrary load of $P = 1\,N$ obtained $\delta\Pi = 2.6685E-5$.

Using (59) with $\Delta H_{11} = 1.656E-3$, $\Delta H_{22} = 5.121E-4$, $\Delta H_{1221} = 8.299E-4$ (from the Tables above and adjusted for the relevant E, ν according to (60)) and $A_1 = 0.73\,\text{MPa mm}^{0.49499}$, $m = 0.09$ (A_1 and A_2 were computed from the sharp V-notch case) we obtained $\delta\Pi = 2.6777E-5$ resulting in a 0.0034% difference. Increasing the crack length to $\ell = 0.066\,\text{mm}$ the resulting difference between the two methods is still less then 0.5%.

6 Comparison with experimental results

To the best of our knowledge, mixed mode loading on V-notch specimens with different notch radii are reported only in Yosibash et al. (2006), Priel et al. (2007). There three point bending (3PB) experiments conducted on PMMA blunt V-notched specimens are detailed. The specimens considered are sets $b1$ and $b2$ having a V-notch opening angle of $\omega = 315^\circ$ and notch tip radii of $a = 0.03$ and $a = 0.25\,\text{mm}$ respectively with $K_{Ic} = 1.12\,\text{MPa}\sqrt{m}$ (averaged value), $E = 3100\,\text{MPa}$, $\nu = 0.36$ and $\sigma_c = 111.8\,\text{MPa}$. In Yosibash et al. (2006), Priel et al. (2007) the failure load and failure initiation angle were predicted by the assumption

Table 3 Mixed mode loading: $H_{ij}(\mu)$ for $\omega = 315°$, $E = 1$, $\nu = 0.3$, $\alpha_1 = 0.5050097$, $\alpha_2 = 0.6597016$, $a = 0.03$, $\rho_1 = 80$, $\rho_2 = 110$, $\rho_\infty = 250$

μ	$H_{11}(\mu)$	$H_{22}(\mu)$	$H_{12}(\mu)$	ΔH_{11}	ΔH_{22}	ΔH_{12}	$\delta\Pi$	$\delta\Pi^{FE}$ (error %)	$h^{mixed}(\mu)$
$\theta^* = 0°$									
0.0	−7.8195	−2.1122	0.0001	0.0000	0.0000	0.0000	0.0000	0.0000 (NA)	0.0000
0.4	−6.5470	−2.1869	0.0000	1.2724	0.0746	−0.0001	0.0198	0.0196 (1.01%)	0.5753
0.6	−5.5572	−2.3532	−0.0001	2.2622	0.2410	−0.0002	0.0353	0.0351 (0.59%)	0.6789
0.8	−4.5035	−2.6278	−0.0001	3.3159	0.5156	−0.0002	0.0517	0.0516 (0.24%)	0.7439
1.0	−3.4177	−3.0050	−0.0001	4.4018	0.8928	−0.0002	0.0686	0.0686 (−0.06%)	0.7881
1.2	−2.3139	−3.4750	−0.0001	5.5055	1.3627	−0.0002	0.0858	0.0861 (−0.33%)	0.8197
2.0	2.1759	−6.1002	0.0000	9.9953	3.9879	−0.0001	0.1557	0.1578 (−1.36%)	0.8876
2.5	5.0047	−8.2093	0.0000	12.8242	6.0971	−0.0001	0.1997	0.2036 (−1.95%)	0.9086
3.0	7.8357	−10.5944	0.0000	15.6552	8.4822	−0.0001	0.2437	0.2500 (−2.54%)	0.9223
3.5	10.6664	−13.2105	0.0000	18.4858	11.0983	−0.0001	0.2877	0.2969 (−3.10%)	0.93178
4.0	13.4933	−16.0253	0.0000	21.3127	13.9131	−0.0001	0.3317	0.3443 (−3.67%)	0.9385
$\theta^* = 5°$									
0.0	−7.8195	−2.1122	0.0001	0.0000	0.0000	0.0000	0.0000	0.0000 (NA)	
0.4	−6.5564	−2.2078	0.3548	1.2630	0.0956	0.3547	0.0200	0.0198 (0.93%)	
0.6	−5.5730	−2.3889	0.6072	2.2465	0.2766	0.6072	0.0356	0.0354 (0.52%)	
0.8	−4.5251	−2.6809	0.8632	3.2944	0.5686	0.8632	0.0521	0.0520 (0.21%)	
1.0	−3.4450	−3.0702	1.1174	4.3744	0.9580	1.1173	0.0692	0.0692(−0.09%)	
1.2	−2.3471	−3.5512	1.3689	5.4723	1.4389	1.3689	0.0865	0.0868 (−0.38%)	
$\theta^* = 10°$									
0.0	−7.8195	−2.1122	0.0001	0.0000	0.0000	0.0000	0.0000	0.0000 (NA)	
0.4	−6.5835	−2.2808	0.6946	1.2360	0.1686	0.6945	0.0199	0.0197 (0.86%)	
0.6	−5.6186	−2.5076	1.1904	2.2008	0.3954	1.1903	0.0354	0.0352 (0.46%)	
0.8	−4.5893	−2.8356	1.6934	3.2302	0.7233	1.6933	0.0518	0.0518 (0.14%)	
1.0	−3.5265	−3.2607	2.1941	4.2930	1.1485	2.1940	0.0688	0.0689 (−0.15%)	
1.2	−2.4448	−3.7744	2.6906	5.3747	1.6621	2.6905	0.0861	0.0865 (−0.42%)	
$\theta^* = 15°$									
0.0	−7.8195	−2.1122	0.0001	0.0000	0.0000	0.0000	0.0000	0.0000 (NA)	
0.4	−6.6273	−2.3948	1.0053	1.1922	0.2825	1.0053	0.0195	0.0193 (0.75%)	
0.6	−5.6933	−2.6857	1.7261	2.1262	0.5734	1.7260	0.0347	0.0345 (0.36%)	
0.8	−4.6933	−3.0801	2.4599	3.1262	0.9679	2.4598	0.0509	0.0508 (0.05%)	
1.0	−3.6587	−3.5627	3.1923	4.1608	1.4504	3.1922	0.0676	0.0678 (−0.21%)	
1.2	−2.6036	−4.1280	3.9205	5.2158	2.0158	3.9204	0.0847	0.0851 (−0.48%)	

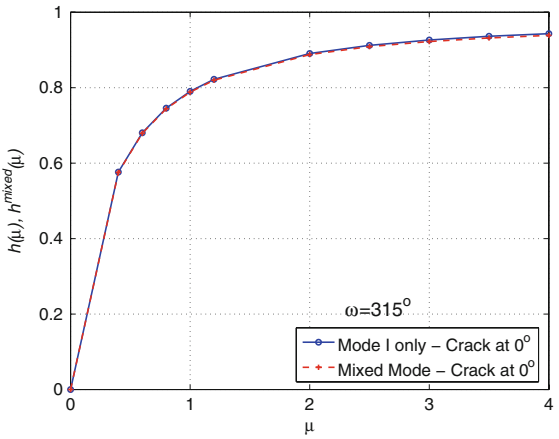

Fig. 12 $h(\mu)$ and $h^{mixed}(\mu, \theta^* = 0)$ for V-notch opening angle of $\omega = 315°$ ($E = 1$, $\nu = 0.3$, $a = 0.03$ mm)

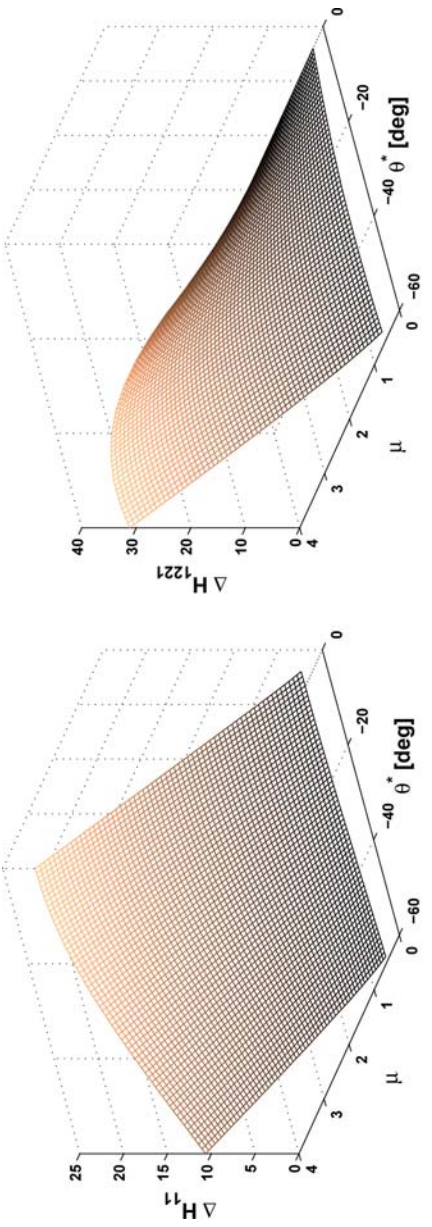

Fig. 13 $\Delta H_{11}(\mu, \theta^*)$, $\Delta H_{22}(\mu, \theta^*)$ and $\Delta H_{12}(\mu, \theta^*)$ for V-notch opening angle of $\omega = 315°$ ($E = 1$, $\nu = 0.3$, $a = 0.03$ mm)

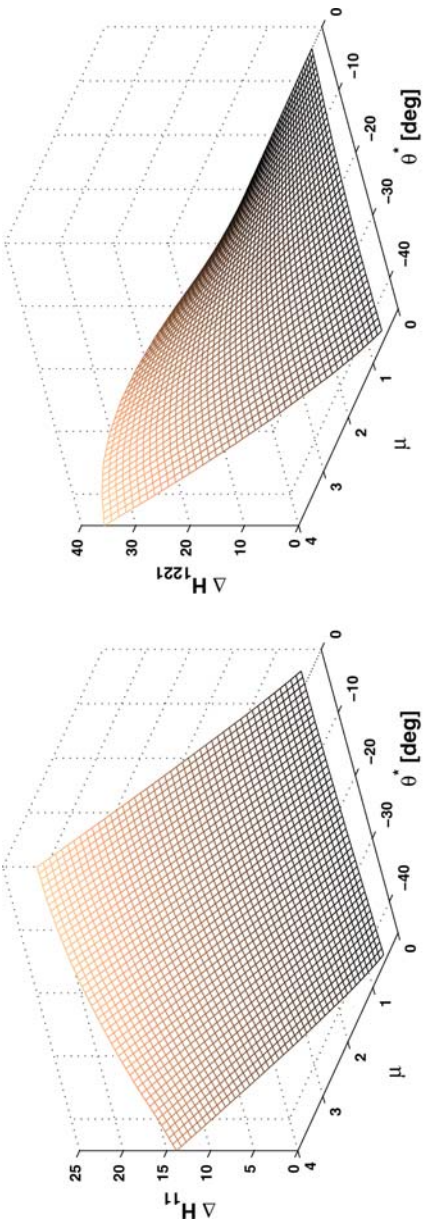

Fig. 14 $\Delta H_{11}(\mu, \theta^*)$, $\Delta H_{22}(\mu, \theta^*)$ and $\Delta H_{12}(\mu, \theta^*)$ for V-notch opening angle of $\omega = 270°$ ($E = 1, \nu = 0.3, a = 0.03\,\text{mm}$)

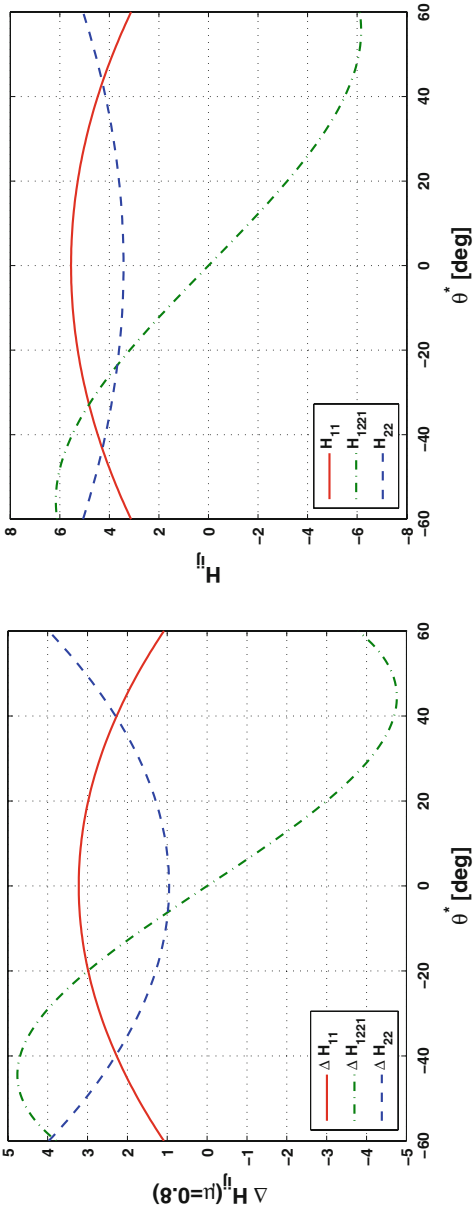

Fig. 15 Comparison between ΔH_{ij} for a blunt notch $\omega = 315°$, $\mu = 0.8$ and H_{ij} for the sharp case $\omega = 315°$

Table 4 Mixed mode loading: $H_{ij}(\mu)$ for $\omega = 315°$, $E = 1$, $\nu = 0.3$, $\alpha_1 = 0.5050097$, $\alpha_2 = 0.6597016$, $a = 0.03$, $\rho_1 = 80$, $\rho_2 = 110$, $\rho_\infty = 250$

μ	$H_{11}(\mu)$	$H_{22}(\mu)$	$H_{12}(\mu)$	ΔH_{11}	ΔH_{22}	ΔH_{12}
$\theta^* = 20°$						
0.0	−7.8195	−2.1122	0.0001	0.0000	0.0000	0.0000
0.4	−6.6995	−2.5384	1.2737	1.1200	0.4262	1.2736
0.6	−5.7933	−2.9203	2.1945	2.0262	0.8081	2.1944
0.8	−4.8338	−3.3932	3.1354	2.9857	1.2810	3.1353
1.0	−3.8368	−3.9531	4.0781	3.9827	1.8409	4.0781
1.2	−2.8187	−4.5885	5.0183	5.0008	2.4763	5.0182
$\theta^* = 25°$						
0.0	−7.8195	−2.1122	0.0001	0.0000	0.0000	0.0000
0.4	−6.4908	−3.4451	3.2095	1.3286	1.3329	3.2094
0.6	−5.9165	−3.1876	2.5788	1.9030	1.0754	2.5788
0.8	−5.0054	−3.7570	3.6975	2.8141	1.6448	3.6974
1.0	−4.0560	−4.4037	4.8238	3.7634	2.2915	4.8237
1.2	−3.0832	−5.1223	5.9509	4.7362	3.0100	5.9508
$\theta^* = 30°$						
0.0	−7.8195	−2.1122	0.0001	0.0000	0.0000	0.0000
0.4	−6.2591	−3.6310	2.7343	1.5603	1.5188	2.7342
0.6	−5.9011	−3.8913	3.2461	1.9184	1.7791	3.2461
0.8	−5.1738	−4.3775	4.2635	2.6457	2.2653	4.2634
1.0	−4.3162	−4.8774	5.5672	3.5033	2.7651	5.5671
1.2	−2.6548	−6.0300	7.3158	5.1646	3.9178	7.3158

of a sharp V-notch, being corrected herein to include the influence of the notch tip radius. Table 7 summarizes the experimental data and the failure loads predicted by the assumption of a sharp V-notch and these predicted including the influence of the notch tip radius.

In Table 7 we computed critical A_{1c}^{blunt} using (70) and A_{1c} using the sharp V-notch criterion reported in Yosibash et al. (2006). We then defined a correction factor to the sharp notch estimation as $\frac{A_{1c}^{blunt}}{A_{1c}}$. Figures 16 and 17 present the correction factors as a function of $\frac{A_2}{A_1}$ and a. The case $\frac{A_2}{A_1} = 0$ is the mode I loading and the value of $\frac{A_{1c}^{blunt}}{A_{1c}} = 1.08$ for $a = 0.03$mm is obtained which is 10% lower compared to the one reported in Fig. 9 (Leguillon and Yosibash 2003)—this is because of the different K_{Ic} values used herein compared to the one in Leguillon and Yosibash (2003).

Using the correction factor we computed the corrected failure load. Prediction results are plotted in Fig. 18.

In all cases the predicted crack initiation angle for the sharp and blunt case were very similar $\pm 1°$.

It can be seen that the correction factor provides better correlation of the predicted values to the experimental observations.

7 Summary and conclusions

Structures containing V-notches fail at significantly lower loads then their material strength would suggest. Predicting the failure load, especially for complex mixed mode state of stresses, has been a topic of active research for the past couple of years. Several failure criteria for predicting the failure load of such structures assuming the V-notch tip is sharp

Table 5 $\Delta H_{11}(\mu,\theta^*)$, $\Delta H_{1221}(\mu,\theta^*)$ and $\Delta H_{22}(\mu,\theta^*)$ for $\omega = 315°$, $E = 1$, $\nu = 0.3$, $\rho_1 = 80$, $\rho_2 = 110$, $\rho_\infty = 250$

μ	−60	−55	−50	−45	−40	−35	−30	−25	−20	−15	−10	−5	0
$\Delta H_{11}(\mu,\theta^*)$													
0	0	0	0	0	0	0	0	0	0	0	0	0	0
0.4	0.41	0.50	0.59	0.69	0.79	0.88	0.98	1.06	1.12	1.19	1.24	1.26	1.27
0.6	0.79	0.95	1.11	1.28	1.44	1.61	1.76	1.90	2.03	2.13	2.20	2.25	2.26
0.8	1.23	1.46	1.69	1.93	2.17	2.40	2.62	2.81	2.99	3.13	3.23	3.29	3.32
1	1.73	2.02	2.32	2.63	2.94	3.23	3.51	3.76	3.98	4.16	4.29	4.37	4.40
1.2	2.25	2.61	2.98	3.36	3.73	4.09	4.43	4.74	5.00	5.22	5.37	5.47	5.51
2	4.52	5.16	5.80	6.45	7.08	7.68	8.24	8.75	9.17	9.53	9.79	9.94	10.00
2.5	6.02	6.82	7.64	8.45	9.24	9.99	10.67	11.29	11.83	12.25	12.57	12.76	12.82
3	7.55	8.52	9.51	10.48	11.42	12.31	13.13	13.86	14.48	14.99	15.35	15.58	15.66
3.5	9.10	10.24	11.39	12.52	13.61	14.63	15.58	16.42	17.14	17.72	18.14	18.40	18.49
4	10.65	11.96	13.27	14.55	15.79	16.96	18.03	18.98	19.79	20.44	20.92	21.21	21.31
$\Delta H_{1221}(\mu,\theta^*)$													
0	0	0	0	0	0	0	0	0	0	0	0	0	0
0.4	1.39	1.55	1.68	1.75	1.78	1.74	1.65	1.49	1.27	1.00	0.69	0.35	9.34E-05
0.6	2.62	2.85	3.03	3.13	3.14	3.05	2.86	2.57	2.19	1.72	1.19	0.60	1.51E-4
0.8	3.98	4.28	4.49	4.60	4.58	4.42	4.13	3.69	3.13	2.45	1.69	0.86	1.50E-4
1	5.45	5.80	6.03	6.12	6.06	5.82	5.40	4.82	4.07	3.19	2.19	1.11	1.56E-4
1.2	6.98	7.37	7.62	7.69	7.56	7.23	6.69	5.95	5.01	3.92	2.69	1.36	1.52E-4
2	13.50	13.92	14.24	14.15	13.73	12.98	11.78	10.33	8.68	6.80	4.65	2.36	5.95E-05
2.5	17.80	18.34	18.52	18.31	17.68	16.62	15.11	13.28	11.11	8.61	5.87	2.97	1.18E-4
3	22.20	22.76	22.88	22.53	21.67	20.31	18.47	16.17	13.47	10.42	7.10	3.60	9.08E-05
3.5	26.68	27.26	27.31	26.80	25.71	24.04	21.81	19.07	15.85	12.25	8.34	4.22	9.12E-05
4	31.20	31.80	31.79	31.12	29.79	27.80	25.19	21.98	18.26	14.10	9.59	4.85	6.32E-05
$\Delta H_{22}(\mu,\theta^*)$													
0	0	0	0	0	0	0	0	0	0	0	0	0	0
0.4	1.21	1.24	1.22	1.16	1.05	0.91	0.75	0.58	0.42	0.28	0.16	0.09	0.07
0.6	2.21	2.23	2.18	2.05	1.86	1.62	1.35	1.07	0.80	0.57	0.39	0.27	0.24
0.8	3.34	3.33	3.22	3.02	2.74	2.40	2.02	1.64	1.28	0.96	0.72	0.56	0.51
1	4.55	4.51	4.34	4.05	3.68	3.25	2.77	2.29	1.84	1.45	1.14	0.95	0.89
1.2	5.84	5.75	5.51	5.15	4.69	4.15	3.58	3.01	2.47	2.01	1.66	1.43	1.36

Table 5 continued

μ	−60	−55	−50	−45	−40	−35	−30	−25	−20	−15	−10	−5	0
2	11.56	11.10	10.75	10.07	9.25	8.35	7.41	6.51	5.53	4.96	4.43	4.107	3.98
2.5	15.51	15.08	14.40	13.52	12.49	11.37	10.08	9.07	8.11	7.27	6.63	6.23	6.09
3	19.71	19.15	18.31	17.23	15.98	14.64	13.29	11.99	10.82	9.83	9.09	8.63	8.48
3.5	24.14	23.45	22.43	21.15	19.70	18.15	16.58	15.09	13.75	12.63	11.79	11.27	11.09
4	28.74	27.92	26.75	25.28	23.61	21.85	20.08	18.40	16.89	15.63	14.69	14.11	13.91

Table 6 $\Delta H_{11}(\mu,\theta^*)$, $\Delta H_{1221}(\mu,\theta^*)$ and $\Delta H_{22}(\mu,\theta^*)$ for $\omega = 270°$, $E = 1, \nu = 0.3$, $\rho_1 = 80$, $\rho_2 = 110$, $\rho_\infty = 250$

μ	−45	−40	−35	−30	−25	−20	−15	−10	−5	0
$\Delta H_{11}(\mu,\theta^*)$										
0	0	0	0	0	0	0	0	0	0	0
0.4	0.50	0.61	0.71	0.81	0.91	0.99	1.06	1.12	1.15	1.16
0.6	0.99	1.16	1.34	1.50	1.66	1.80	1.91	1.99	2.05	2.06
0.8	1.56	1.80	2.04	2.28	2.49	2.68	2.83	2.94	3.01	3.04
1	2.18	2.50	2.81	3.10	3.37	3.60	3.80	3.94	4.03	4.06
1.2	2.85	3.23	3.61	3.97	4.29	4.57	4.79	4.96	5.07	5.10
2	5.77	6.43	7.07	7.65	8.18	8.63	8.99	9.26	9.42	9.48
2.5	7.74	8.56	9.35	10.07	10.72	11.28	11.72	12.05	12.25	12.31
3	9.76	10.74	11.68	12.55	13.32	13.98	14.50	14.89	15.12	15.20
3.5	11.83	12.94	14.06	15.07	15.96	16.72	17.32	17.77	18.04	18.13
4	13.92	15.07	16.44	17.62	18.63	19.49	20.18	20.68	20.98	21.08
$\Delta H_{1221}(\mu,\theta^*)$										
0	0	0	0	0	0	0	0	0	0	0
0.4	1.21	1.30	1.35	1.34	1.24	1.09	0.87	0.60	0.29	0.01
0.6	2.35	2.45	2.48	2.40	2.22	1.93	1.540	1.07	0.55	0.021
0.8	3.66	3.77	3.75	3.58	3.28	2.82	2.24	1.55	0.79	0.024
1	5.10	5.19	5.11	4.85	4.39	3.76	2.97	2.05	1.049	0.02
1.2	6.64	6.71	6.56	6.17	5.56	4.74	3.73	2.58	1.31	0.02
2	13.72	13.59	13.02	12.05	10.72	9.04	7.05	4.83	2.45	0.004
2.5	18.68	18.39	17.53	16.15	14.30	12.00	9.34	6.39	3.24	0.005
3	24.04	23.56	22.36	20.52	18.12	15.18	11.79	8.05	4.08	0.007
3.5	29.78	29.02	27.48	25.16	22.16	18.52	14.37	9.81	4.96	0.019
4	35.82	34.69	32.86	30.04	26.41	22.05	17.08	11.64	5.88	0.026
$\Delta H_{22}(\mu,\theta^*)$										
0	0	0	0	0	0	0	0	0	0	0
0.4	0.92	0.92	0.79	0.78	0.62	0.53	0.43	0.32	0.22	0.22
0.6	1.63	1.56	1.30	1.28	0.89	0.73	0.46	0.33	0.23	0.23
0.8	2.47	2.36	2.14	1.90	1.36	1.13	0.95	0.62	0.50	0.45
1	3.46	3.27	2.91	2.47	2.16	1.64	1.27	1.03	0.87	0.82
1.2	4.55	4.31	3.89	3.27	2.86	2.26	1.90	1.62	1.35	1.30
2	10.21	9.50	8.80	7.83	6.79	6.04	5.17	4.66	4.35	4.27
2.5	15.07	13.83	12.78	11.43	10.33	9.08	8.16	7.34	6.94	6.80
3	20.14	18.71	17.33	15.82	14.25	12.73	11.59	10.73	10.09	9.93
3.5	25.98	24.31	22.63	20.80	18.93	17.17	15.59	14.53	13.80	13.57
4	32.53	30.59	28.51	26.43	24.16	22.08	20.39	18.92	18.31	17.95

Table 7 Dimensions, experimental and predicted failure loads for 3PB PMMA specimens $\omega = 315°$

Specimen	Configuration (mm)			L/H/b (mm)	Failure load (N)			θ_i Exp (°)
#	xp	$xs1$	$xs2$	b = thickness	Exp	Sharp prediction	Blunt prediction	
b1-2	2	18	22	80 × 10 × 10	317	183	250	85
b1-3	6	14	26	80 × 10 × 10	327	231	313	80
b1-4	10	10	30	80 × 10 × 10	533	329	438	68
b1-5	13.5	6.5	33.5	80 × 10 × 10	744	500	648	60
b1-6	16	4	36	80 × 10 × 10	1280	824	993	50
b2-2	2	18	22	80 × 10 × 10	226	183	215	85
b2-3	6	14	26	80 × 10 × 10	301	231	264	79
b2-4	10	10	30	80 × 10 × 10	408	329	378	72
b2-5	13.5	6.5	33.5	80 × 10 × 10	613	500	565	68
b2-6	16	4	36	80 × 10 × 10	998	824	905	60

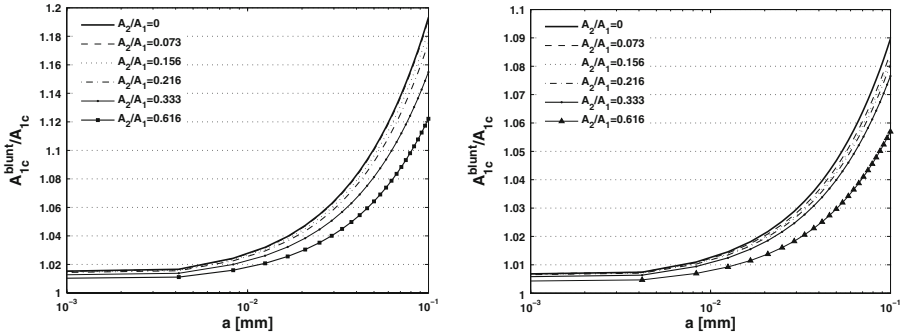

Fig. 16 Correction factor for PMMA as a function of the notch tip radius: Left—$\omega = 315°$ (A_2/A_1 dimension is $\text{mm}^{-0.154}$) Right- $\omega = 270°$ (A_2/A_1 dimension is $\text{mm}^{-0.364}$)

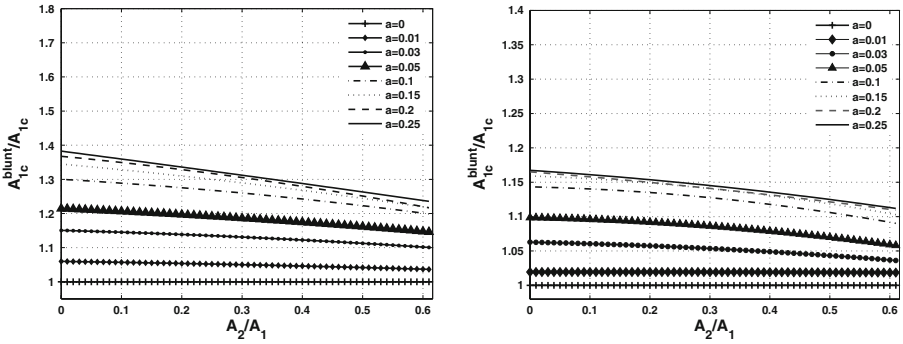

Fig. 17 Correction factor for PMMA as a function of the mode mixity: Left—$\omega = 315°$ (A_2/A_1 dimension is $\text{mm}^{-0.154}$), Right- $\omega = 270°$ (A_2/A_1 dimension is $\text{mm}^{-0.364}$)

have been presented for mixed mode I and II loading. Actual V-notches are never sharp but when the V-notch tip radius is small $a \leq 0.01\,\text{mm}$ some mixed mode sharp V-notch criteria provide accurate predictions of the failure load. As the V-notch tip radius increases their accuracy deteriorates and correction factors accounting for this V-notch tip radius are required. Such correction factors have been reported for the simpler case of pure mode I loading but to the best of our knowledge none exist for mixed mode cases.

Herein we presented a method to compute correction factors to the critical load predicted by the sharp V-notch mixed mode failure criterion reported in Yosibash et al. (2006). The correction factor is influenced by both the V-notch tip radius and the mixed mode state of loading. It has been demonstrated that the sharp V-notch criterion presented in Yosibash et al. (2006) is the limiting case where the V-notch tip radius $a \to 0$. Using mixed mode experimental data reported in Priel et al. (2007) on PMMA we demonstrate that the correction brings the predicted sharp V-notch values closer to the experimental observations (Fig. 18). The remaining discrepancy is probably due to micro-mechanisms neglected in this analysis (as plastic effects, etc).

From our analysis it is apparent (16) that the correction factor needed for a fixed V-notch tip radius decreases as the mode mixity increases. We obtain the same drop in correction factor values when we compute the correction factor for increasing values of V-notch opening angle, be it for mixed mode or pure mode I loading. This phenomenon can be attributed

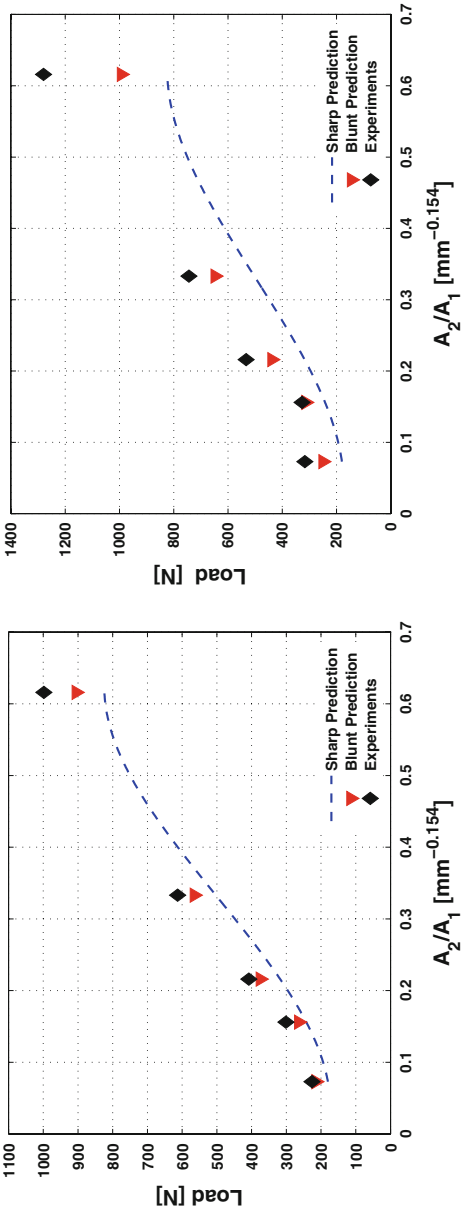

Fig. 18 Experimental and predicted values for PMMA specimens: Left—Set $b1$ ($a = 0.03$ mm) Right—Set $b2$ ($a = 0.25$ mm)

to the drop in the mode I singular stress field which decreases for raising values of mode mixity and/or increasing value of V-notch tip radii. It is demonstrated in Fig. 16 that for small V-notch tip radii ($a \leq 0.01$ mm for the PMMA analyzed in this paper) no correction is needed and the sharp mixed mode criterion is sufficient to accurately predict the critical load. When one considers relatively large V-notch tip radii the accuracy of the proposed correction factor deteriorates because the formulation of the criterion is based on the smallness of the V-notch tip radius allowing an asymptotic analysis.

Acknowledgements The first two authors gratefully acknowledge the support of this research by the VATAT-VEE (grant No. 86/07) and by the Israel Science Foundation (grant No. 750/07). Special thanks are extended to Mr. Nir Trabelsi at the Computational Mechanics Laboratory, Ben-Gurion University, Beer-Sheva, Israel for his assistance with the Matlab code.

References

Gomez FJ, Elices M (2004) A fracture criterion for blunted v-notched samples. Int J Fract 127:239–264

Gomez FJ, Elices M, Berto F, Lazzarin P (2007) Local strain energy to assess the static failure of u-notches in plates under mixed mode loading. Int J Fract 145:29–45

Kanninen MF, Popelar CH (1985) Advanced fracture mechanics. Oxford University Press, New York

Lazzarin P, Berto F (2005) Some expressions for the strain energy in a finite volume surrounding the root of blunt v-notches. Int J Fract 135:161–185

Lazzarin P, Tovo R (1996) A unified approach to the evaluation of linear elastic fields in the neighborhood of notches. Int J Fract 78:3–19

Leguillon D (2002) Strength or toughness? A criterion for crack onset at a notch. Eur J Mech A/Solids 21:61–72

Leguillon D, Yosibash Z (2003) Crack onset at a v-notch. Influence of the notch tip radius. Int J Fract 122:1–21

Leguillon D, Laurencin J, Dupeux M (2003) Failure initiation in an epoxy joint between two steel plates. Eur J Mech A/Solids 22(4):509–524

Priel E, Bussiba A, Gilad I, Yosibash Z (2007) Mixed mode failure criteria for brittle elastic v-notched structures. Int J Fract 144:247–265

Szabó BA, Babuška I (1988) Computation of the amplitude of stress singular terms for cracks and reentrant corners. In: Cruse TA (ed) Fracture mechanics: nineteenth symposium. ASTM STP 969, ASTM, Philadelphia pp 101–124

Szabó BA, Babuška I (1991) Finite element analysis. Wiley, New York

Williams ML (1952) Stress singularities resulting from various boundary conditions in angular corners of plates in extension. Trans ASME J Appl Mech 19:526–528

Yosibash Z, Bussiba A, Gilad I (2004) Failure criteria for brittle elastic materials. Int J Fract 125(3–4):307–333

Yosibash Z, Priel E, Leguillon D (2006) A failure criterion for brittle elastic materials under mixed-mode loading. Int J Fract 141(1):291–312